



**Proyecto Final de Estudios
MÁSTER
EN
INGENIERÍA BIOMÉDICA**

EB

**Characterization of Intracranial Aneurysms in Middle
Cerebral Artery (MCA)**

Barcelona, 3 de Marzo de 2010

Autor: Carolina Valencia Muñoz

Director: Carles Falcon Falcon

Tutores: Mari Cruz Villa Uriol

Alejandro F. Frangi

Realizado en: Computational Imaging and Simulation
Technologies in Biomedicine (CISTIB)
Universitat Pompeu Fabra



Data de registre:

MÀSTER ENGINYERIA BIOMÈDICA

Registre Projecte Final d'Estudis

NOM DE L'ALUMNE: Carolina Valencia Muñoz

TÍTOL DEL PROJECTE: Characterization of Intracranial Aneurysms in Middle Cerebral Artery (MCA)

DIRECTOR/S DEL PROJECTE:
(Indiqueu Centre, Departament, Empresa, Hospital, etc. on està vinculat el director)

Maria Cruz Villa Urid - Computational Imaging and Simulation Technologies in Biomedicine (CISTIB) - Universitat Pompeu Fabra

Alejandro Frangi - Computational Imaging and Simulation Technologies in Biomedicine (CISTIB) - Universitat Pompeu Fabra

Carles falcon falcon -Unitat de Biotècnica y Bioingenieria - Depto de Ciències fisiològiques I - Universitat de Barcelona

Dr. Director del projecte

Dr. Pere Caminal
Coordinador UPC
Màster Enginyeria Biomèdica

Carolina Valencia Muñoz
Signatura de l'alumne

Dr. Josep Samitier
Coordinador UB
Màster Enginyeria Biomèdica

Resumen

Los aneurismas intracraneales han sido el objetivo de muchos investigadores, pero a pesar de haber encontrado múltiples correlaciones entre la ruptura del aneurisma y los factores de riesgo, su estudio sigue siendo limitado. Ya que la morfología de aneurismas cerebrales ha sido considerada como un potencial suplente de ruptura, en este proyecto la influencia de variables morfológicas en la ruptura del aneurisma ha sido estudiada. Entre las características morfológicas propuestas, diversos índices han permitido establecer vínculos con el riesgo de ruptura para una lesión específica. Estos podrían conducir a una mejor comprensión de los mecanismos de ruptura de aneurisma cerebral.

Este estudio se presenta una completa y eficiente metodología basada en imágenes para el análisis de aneurismas cerebrales específicos del paciente, incluyendo el saco y las arterias adyacentes. Esta metodología permite al modelado de un número elevado de aneurismas de una manera eficiente para obtener un modelo específico de la geometría del aneurisma del paciente. La metodología emplea algoritmos que iniciando desde las imágenes de Angiografía Rotatoria Tridimensional (3DRA), creando un modelo de malla que morfológicamente es procesado produciendo un número de medidas básicas de forma así como medidas más sofisticadas como los Momentos de Zernike. Estos cálculos han sido realizados sobre una población de 95 aneurismas rotos y no rotos (79 pacientes) localizados en la Arteria Cerebral Media (MCA).

Entre el conjunto de índices calculados, estudios estadísticos muestran que entre más información tridimensional los descriptores morfológicos contienen, más robusto discriminan entre aneurismas rotos y no rotos. Éste es el caso para los Momentos de Zernike basados en el volumen, que proporcionaron los mejores resultados de predicción en comparación con otros descriptores como el índice de no esfericidad.

Abstract

Intracranial aneurysms have been the aim of many researchers, but despite finding multiple correlations between aneurysm rupture and risk factors, their study still remains limited. Since cerebral aneurysms morphology has been considered as a potential surrogate of rupture, in this project the influence of morphological variables in the aneurysm's rupture have been studied. Among the proposed morphological characteristics, several indices have allowed to establish links between these descriptors and the risk of rupture for a specific lesion. These might lead to a better understanding of the cerebral aneurysm rupture mechanisms.

This study presents a complete and efficient image-based methodology for the analysis of cerebral aneurysms on a patient-specific basis including the sac and the parent vessel. This methodology allows the modeling of a large number of aneurysms in a time-efficient manner to obtain a patient-specific model of the aneurysm geometry. Our pipeline uses algorithms that starting from Three-Dimensional Rotational Angiography (3DRA) images create a mesh model that is morphologically processed producing a number of basic shape measurements as well as most sophisticated ones such as the Zernike Moments. These computations have been performed on a population of 95 ruptured and unruptured aneurysms (79 patients) located at the Middle Cerebral Artery (MCA).

Among the set of computed indices, statistical studies show that the more tridimensional information the morphological descriptors contain, the more robust they are discriminating between ruptured and unruptured aneurysms. This is the case for volume-based Zernike moments, which provided the best prediction results compared to other descriptors such as the Non-Sphericity Index.

Table of Contents

Resumen.....	1
Abstract.....	3
Table of Contents.....	5
Abbreviations.....	7
Introduction.....	9
Chapter I Background and Objectives.....	11
I.1. Cerebral vasculature.....	11
I.1.1. Circle of Willis.....	12
I.2. Cerebral Aneurysms.....	13
I.2.1. Classification and Risk Factors.....	13
I.2.2. Symptoms and Diagnosis.....	16
I.2.3. Treatment and therapies.....	16
I.3. Imaging techniques.....	18
I.3.1. Computed Tomography Angiography (CTA).....	18
I.3.2. Magnetic Resonance Angiography (MRA).....	18
I.3.3. Three-Dimensional Rotational Angiography (3DRA).....	18
I.4. Image-based Modeling.....	20
I.5. Morphological Characterization: Literature Overview.....	22
I.6. Objectives.....	29
Chapter II Materials and Methods.....	30
II.1. Patient Population.....	30

II.2. Reconstructed Models.....	30
II.2.1. Image Data.....	31
II.2.2. Image segmentation.....	31
II.2.3. Surface meshing.....	32
II.2.4. Skeleton.....	32
II.2.5. Isolation of the model.....	32
II.3. Morphological Characterization.....	33
II.3.1. Size indices.....	33
II.3.2. Shape indices.....	33
II.4. Statistical analysis.....	35
II.4.1. Linear Discriminant Analysis (LDA).....	36
II.4.2. Principal Components Analysis (PCA).....	37
II.4.3. Receiver Operating Curves (ROC).....	37
Chapter III Results.....	38
Chapter IV Discussion and Limitations.....	43
Chapter V Conclusions and Further work.....	45
Acknowledgements.....	47
List of figures.....	48
List of tables.....	49
Bibliography.....	50

Abbreviations

2D	Two-dimensional
3D	Three-dimensional
ACA	Anterior cerebral artery
AcomA	Anterior communicating artery
AICA	Anterior inferior cerebellar artery
BA	Basilar artery
CFD	Computational Fluid Dynamics
CTA	Computed Tomography Angiography
DSA	Digital Subtraction Angiography
GDCs	Guglielmi detachable coils
ICA	Internal carotid artery
IEL	Internal elastic lamina
IA	Intracranial Aneurysms
ISAT	International Subarachnoid Aneurysm Trial
ISUIA	International Study of Unruptured Intracranial Aneurysms
MIP	Maximum Intensity Projection
MRA	Magnetic Resonance Angiography
PCA	Posterior cerebral artery
PC	Phase Contrast
PcomA	Posterior communicating artery
PICA	Posterior inferior cerebellar artery
ROI	Region of Interest
SAH	Subarachnoid hemorrhage
SCAA	Saccular cerebral artery aneurysm
TOF	Time of Flight
WSS	Wall Shear Stress

Introduction

Saccular intracranial aneurysms are localized enlargement lesions of the vasculature, most commonly located at bifurcation points in the circle of Willis (Brisman *et al.* 2006). Their prevalence is about 1 to 5 percent in adult population (Wiebers *et al.* 2003). Often they will stay asymptomatic during the course of life (Connolly and Solomon 1998), but their rupture constitute the main cause known of the subarachnoid hemorrhage (SAH), which causes high morbidity and mortality rates (Johnston *et al.* 1998).

The current advances in medical imaging and especially the advent of three-dimensional rotational angiography (3DRA) have introduced a significant change in the diagnosis, treatment planning and outcome control of cerebrovascular diseases. These developments in neuroradiological imaging have allowed an increasing discovery of incidental unruptured aneurysms (Yasui *et al.* 1998), therefore an increasing of the preventive treatment. These techniques also provide information to create computer models of the cerebral vasculature, in order to obtain 3D information on vessel morphology and extract possible factors associated with a high risk of rupture.

The numerous characteristics studied include aneurysm and patient-specific information, and their aim is to support the clinical management of these lesions. Aneurysm-related risk factors include location and size and morphological features such as the shape of the aneurysm and other patient-related risk factors such as genetics, gender, age, hypertension, smoking and alcohol habits. Linking such new indices with relevant clinical events should bring new insights on the processes behind aneurysm genesis, growth and rupture. If implemented an automatic method to quantify and to characterize the shape of aneurysms, it could potentially provide robust criteria to assess the risk of aneurysm rupture.

The objective of this work is to morphologically characterize intracranial aneurysms using image-based techniques that provide a patient-specific model allowing to extract relevant information from which prognostic descriptors can be obtained. The combination of all these factors might give rise to particular conditions inducing the formation, growth and rupture of aneurysms.

Chapter I Background and Objectives

I.1. Cerebral vasculature

The cerebral circulation system is a tree of blood vessels, veins and arteries, which irrigate the brain, represent the two percent of the body weight and receive one-fifth of the total cardiac output (Eymann 2004). The diameter of the vessels, which is around of 1 cm in the internal carotid, becomes narrower in the branching, reaching 0,5 cm in the small arteries and about 0,001 cm in the microcapillars. The arterial wall is generally composed of three major layers. Going from the innermost layer closest to the lumen towards the outer side, they are called respectively: endothelium or intima, muscular media and adventia (Stehbens 1972).

In a healthy human, the carotid arteries are the main blood supply to the brain, feeding the majority of the cerebrum and vertebral circulation. The circulation can be classified anatomically into anterior and posterior circulation (Eymann 2004).

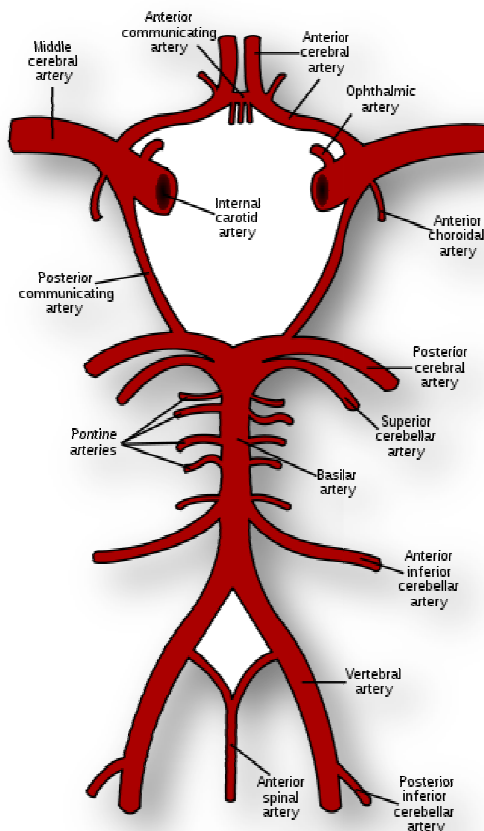
The left and right internal carotid arteries arise from the right and left common carotid arteries at the C4 vertebra, to supply the anterior circulation of the brain. The internal carotid artery becomes the anterior cerebral artery (ACA) and the middle cerebral artery (MCA). The ACA carries blood to the frontal parietal and a small part of the occipital lobe. The anterior communicating artery connects the two anterior cerebral arteries and the posterior communicating artery are branches of the internal carotid artery. All arteries involved give off cortical and central branches. The MCA is the largest branch of the internal carotid artery and is one of the three major paired arteries that supplies blood to the cerebrum.

The vertebral arteries of the both sides arise from the subclavian arteries and become one trunk called basilar artery which supplies the posterior circulation of the brain including the cerebellar and posterior meningeal arteries. From the Basilar artery, the two posterior cerebral arteries (PCA) are born. Branches of the Basilar and PCA supply the occipital lobe, brain stem, and the cerebellum. The right and left posterior cerebral arteries arise from the basilar artery, which is formed by the left and right vertebral arteries.

I.1.1. Circle of Willis

Also called the cerebral arterial circle, arterial circle of Willis or Willis Polygon, is a ring at the base of the brain formed by a group of arteries: anterior, middle, posterior and communicating from the left and right side (See Figure I.1). These arteries and their branches are located within the cerebrospinal fluid-filled subarachnoid space and supply blood to the brain. It is named after its discovery by the English physician Thomas Willis (1621–1673). The basilar artery and middle cerebral arteries are not considered part of the circle, even if they supply the brain (Moore and Dalley 1999).

Moreover, this unique structure has the natural capacity to create a by-pass in case of occlusion of one of its branches, therefore establishing a mechanism for the cerebral blood flow auto regulation (Franco Folino 2007). On the other hand, considerable anatomic variations have been found in the circle of Willis. Based on a study of 1413 brains, the classic anatomy of the circle is only observed in 34.5% of the cases (Stehbens 1963). These



anatomical variations include asymmetric branches and sharp bifurcations, and were more frequently found in patients with aneurysms (Kayembe *et al.* 1984). For instance, relatively pointed angles can locally induce disturbed flow and high wall shear stress on the vascular wall causing a dilatation. These hemodynamic properties are indirectly associated with the development of aneurysms (Moritake *et al.* 1976). This motivates the hypothesis that particular hemodynamic conditions – induced by these anatomical variations – might be related to an increased risk of formation, growth and rupture of aneurysms

of the Circle of Willis
| Rhcastilhos 2007.

I.2. Cerebral Aneurysms

Aneurysms are a vascular disease in which an abnormal expansion appears in an artery or vein (Figure I.2). These defects are thought to be caused by a degeneration and weakness in the elastic cap of the internal wall (Frosen *et al.* 2004). The defective collagen, especially at the weak branching points of arteries give rise to easy tearing with a minimal rise in blood pressure. If bleeding occurs during this process, the resulting effect is a hemorrhagic stroke, other complications or even death. This hemorrhage could be presented in the form of **subarachnoid hemorrhage** (subarachnoid space between the brain and the surrounding meninges) or **intracerebral hemorrhage** (brain parenchyma) or both, even though SAH is more frequent.

One third of the SAH patients die before arriving to the hospital, one third of those who are hospitalized will die later, representing an approximate 50% mortality of these cases (Hop *et al.* 1997). Less than half of the survivors suffers severe neurological damage or goes back to normal (around 20% of the initial population) (Van Gijn and Rinkel 2001).

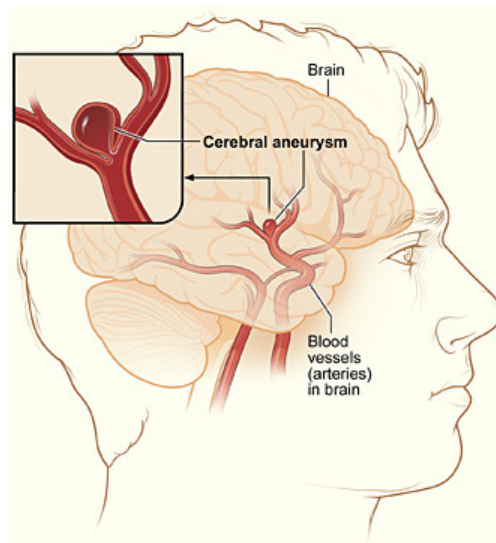


Figure I.2. Aneurysm appearance. Taken from National Heart 2010.

I.2.1. Classification and Risk Factors

In general, aneurysms are classified according to their size, shape, location, vessel type, origin, and other diseases present (Eymann 2004). Furthermore, this discrimination is somehow related with the risk of rupture. Risk factors can be divided into those directly related to the aneurysm and to those related to the patient (Frosen 2006).

According to their size, defined as the maximum length from the neck to the dome, a small aneurysm is considered to be less than 10mm and is the most common size representing a 79% of the entire population; while a large aneurysm has a diameter above 10mm and represents a reduced part of the population (19%). Lesions above 25mm in diameter are commonly call giant aneurysms and represent only the 2%. The latter ones are a huge challenge in terms of treatment to neurosurgeons (Nien *et al.* 2002).

Depending on their shape, aneurysms are described as either "saccular" (berry with a narrow or broad neck) or "fusiform" (resembling a narrow cylinder). Saccular aneurysms are the most common ones and have a more or less spherical shape with an identifiable neck. Fusiform include the entire vessel without an evident neck. Mycotic aneurysms result from a fungal or bacterial infection and are extremely rare (See Figure I.3).

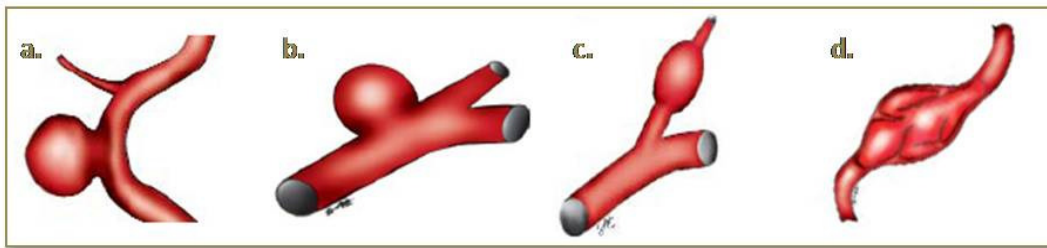


Figure I.3. Types of aneurysms a. Saccular b. Saccular wide neck c. Fusiform d. Mycotic; Adapted from Eymann 2004.

Controversy exists regarding the prevalence of unruptured intracranial aneurysms. Some studies report rates as high as 6.5% in the general population harboring these lesions (Nakagawa and Hashi 1994). However, the vast experience of the neurovascular community would declare these estimates likely to be too elevated (Rinkel 2008).

Regarding the location, the most frequent is in the circle of Willis at bifurcation points, around 85 % of cerebral aneurysms occur in the anterior circulation (Schievink 1997) distributed more or less equal in Internal Carotid, Anterior communicating and middle cerebral arteries. The remaining percent occurs in the posterior circulation at the bifurcation with the basilar or vertebral arteries (See Figure I.4).

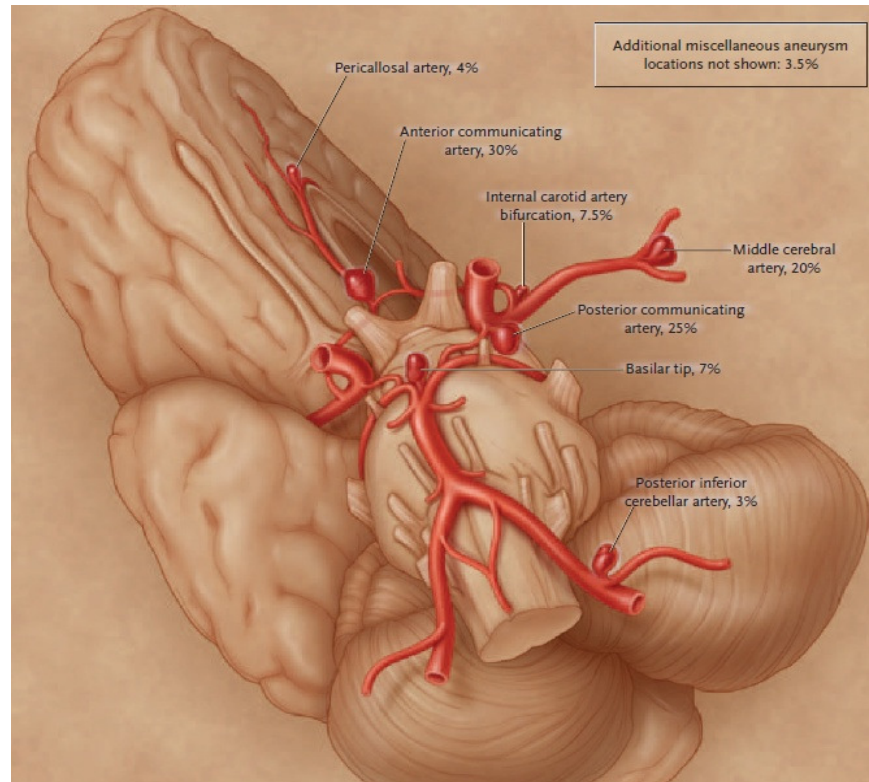


Figure I.4. Frequent Locations and Incidence of Intracranial aneurysms. Taken from Brisman et al. 2006.

Regarding the risk factor related to the patient, currently clinicians include relevant data from the patient such as patient's age, sex, smoking and alcohol habits and familial background. For women are more frequent than for men, by a ratio of 2 to 1 (Brisman et al. 2006). Aneurysms can be classified by the underlying condition, patients with autosomal dominant polycystic kidney disease, a familial predisposition or atherosclerosis which suggests a higher prevalence (Malek *et al.* 1999). For instance, while most aneurysms occur in an isolated form, the occurrence of berry aneurysms of the anterior communicating artery of the circle of Willis is associated with autosomal dominant polycystic kidney disease (ADPKD) (Yanaka *et al.* 2004).

About the vessel type, the two main groups of aneurysms are the abdominal aortic aneurysms and the intracranial aneurysms. Also, vessel type refers to arterial or venous. Arterial aneurysms are more common, but venous aneurysms do happen. This study will focus only in cerebral arterial aneurysms. Finally, growth, large size, secondary pouches or irregular shape are frequently associated with ruptured aneurysms (Raghavan *et al.* 2005).

I.2.2. Symptoms and Diagnosis

Many patients do not realize that they have an aneurysm until it ruptures, which causes bleeding in the brain. The typical symptom of a ruptured aneurysm is the development of a headache described by the patient as the worst had ever had (Brisman et al. 2006). Diagnosis is commonly made by finding signs of subarachnoid hemorrhage or by chance during examinations on a scanner such as computed tomography (CT scan), magnetic resonance imaging (MRI), or angiography.

Symptoms are commonly different according to the location, size and ruptured status of the aneurysm (Menghini *et al.* 2001). Regarding the location, for instance, if the aneurysm is in the ophthalmic segment could be detected by a loss of sight. Regarding the size, small aneurysms generally will not show symptoms (Van Gijn and Rinkel 2001). Whereas, larger aneurysms can put pressure on nerves and tissues. Regarding the ruptured status, an aneurysm unruptured presents signs that include double vision, loss of sight, eye and neck pain and warning headaches (Juvela 1992). These are caused by leakage of blood into the brain for days up to weeks prior to the aneurysm's rupture. For ruptured aneurysm, signs are: sudden severe headache, lethargy, confusion, stupor, seizures, unexpected mood swings, speech impediment, eyelids dropping and movement disorders.

I.2.3. Treatment and therapies

Emergency treatment for patients with a ruptured cerebral aneurysm is usually performed within the first hours after bleeding to occlude it and reduce the risk of rebleeding. For patients with unruptured aneurysms are typically found accidentally during routine check-up or in the case of ruptured of one lesion in a patient with multiple aneurysms. A comparative risk assessment of treatment versus rupture has to be performed.

Many factors are considered when making treatment decisions. The size and location of the aneurysm, the presence of symptoms, the patient's age and medical condition, and other risk factors for aneurysm rupture are considered. In some cases, the lesion may not be treated but the patient will be closely followed by a physician. In other cases, treatment may be indicated. Currently there are two treatment options: surgical clipping or endovascular coiling. Both methods have significant risks and are expensive. Moreover, it seems that the risks associated with surgical clipping and endovascular coiling, in terms of stroke or death from the procedure, are the same (Raja *et al.* 2008).

Surgical clipping is the traditional treatment for aneurysm was introduced by Walter Dandy of the Johns Hopkins Hospital in 1937 (Dandy and Schlesinger 1944). It consists of performing a craniotomy, exposing the aneurysm, isolating it from the circulation by placement of a clip across the neck of the aneurysm (See Figure I.5.a.) The technique has been modified and improved over the years and currently is considered with a lower rate of aneurysm recurrence after treatment. In a systematic review, Raaymakers *et al.* 1998 included 61 studies that involved 2460 patients concluded that the mortality after clipping of unruptured aneurysms is 2.6% and the permanent morbidity is 10.9%.

Endovascular coiling was introduced by Guido Guglielmi *et al.* 1991 at UCLA, has been used increasingly because is much less invasive method. It consists of passing a catheter for a small incision, into the femoral artery until the brain arteries, to reach the aneurysm itself while monitoring with angiographic techniques. Once the catheter is in the aneurysm, platinum coils are pushed into the aneurysm and released (See Figure I.5.b.). These coils initiate a clotting or thrombotic reaction within the aneurysm that, if successful, will eliminate the aneurysm. Therefore, it appears that although is associated with a shorter recovery period as in comparison to surgical clipping. The major problem associated, however, is a higher aneurysm recurrence rate. For instance, Piotin *et al.* 2007 indicate that 28.6% of aneurysms recurred within one year of coiling, and that the recurrence rate increased with time. Moreover, recurrence rate are different regarding their size which 31.1% for small aneurysms less than 10 mm, and 56.0% for aneurysms 10 mm or larger (Piotin *et al.* 2009).

In the case of broad-based aneurysms, a stent may be passed first into the parent artery to serve as a scaffold for the coils ("stent-assisted coiling" See Figure I.5.c.), although the long-term studies of patients with intracranial stents have not yet been done.

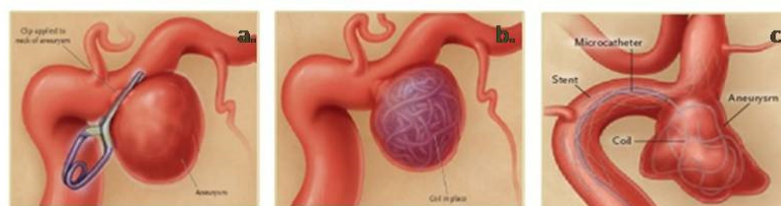


Figure I.5. Current treatments available for intracranial aneurysms. a. Clipping. b. Coiling. c. Stent-assisted coiling. Adapted from Brisman *et al.* 2006.

I.3. Imaging techniques

At present, three imaging modalities allow to identify or rule out an intracranial aneurysm are computed tomography angiography (CTA), magnetic resonance angiography (MRA), and three-dimensional rotational angiography (3DRA).

I.3.1. Computed Tomography Angiography (CTA)

CTA is a technique based on the interpolation of X-ray data. After a contrast agent injection, the head is scanned in spiral with X-Rays. This captures the density around any point of the head. It is less invasive and quicker but is considered less reliable because the image may be disturbed by artifacts from the prominences of the skull base being a problem for diagnosis purposes (McKinney *et al.* 2008). For surgical planning is useful because it can be visualized the vasculature location relative to the brain and the bones.

I.3.2. Magnetic Resonance Angiography (MRA)

MRA removes the signal produced by stationary tissues and detects the presence of fluids. It registers the averaging density around a point of the fluid, giving direct information of the intravascular region. Two types of MRA exist: Phase-contrast (PC) and Time of Flight (TOF). The PC technique gives the density as well the internal velocity in the vessels while the TOF registers only the presence of flow. It is the least invasive method of cerebral angiography, but may produce false negative findings (Vanninen *et al.* 1996). Because of its non-invasive nature, MRA is very useful in follow-up study of treated aneurysms. Given the less invasive nature of CTA and MRA, these two modalities are used in standard clinical practice at early diagnostic stages as well as for patient screening and monitoring (Brisman *et al.* 2006).

I.3.3. Three-Dimensional Rotational Angiography (3DRA)

Finally, 3DRA involves the acquisition of x-ray angiographic images over an arc capturing two consecutive image projections of the patient: before and after the injection of contrast agent. The subsequent reconstruction of these images into a 3D volume, enables to obtain information about morphology of the vessels. Since the reconstruction produces a 3D volume, vessels can be viewed from arbitrary angles (Anxionnat *et al.* 2001). Is the gold standard of cerebral angiography, because provides the highest spatial resolution (Poethke *et al.* 2008). Is used during endovascular treatment, however is the most invasive method.

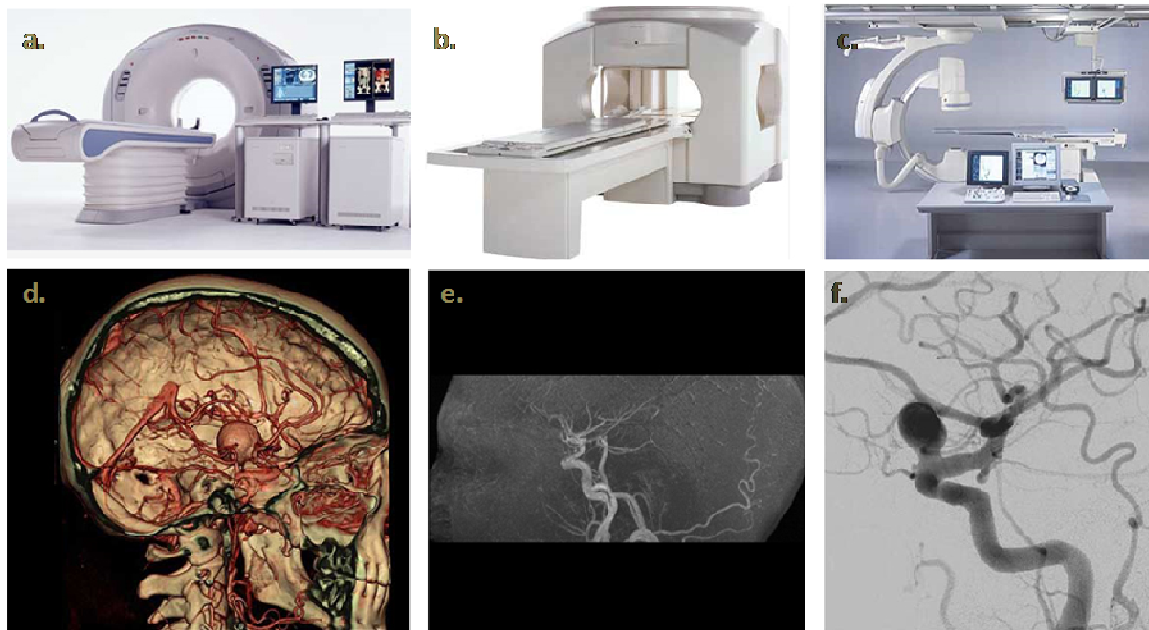


Figure I.6. Different image acquisition modalities a), b) and c) CTA, MRA and 3DRA equipments d), e) and f) different images from the respective modality. Adapted from Radiological Society of North America 2008.

In addition to a complete medical history and physical examination, diagnostic procedures for a cerebral aneurysm may include some limited hemodynamic variables such as pressure, could be obtained with intravascular probes and ultrasound Doppler.

These new approaches allow a better 3D perception of anatomical structures allowing delineating size and morphologic features and showing exactly how blood flows into the brain arteries. This important information allows quantifying parameters for surgical planning. However, none of the currently available image modalities can reliably identify those intracranial aneurysms which will rupture and cannot detect structural weakness or pathobiological changes (wall mechanical properties) or detailed description of hemodynamics that lead to rupture.

I.4. Image-based Modeling

Currently, in vivo or in vitro studies cannot provide complete information of all characteristics of the aneurysms (Castro *et al.* 2006). For that reason, researchers have began to explore computational models that can simulate any possible vascular geometry (Steinman 2002; Hassan *et al.* 2004). This method requires the extraction of features and meaningful information for attempt to derive the geometry and appearance of the scene from multiple real images. Therefore, this technique provides an attractive way for study the geometric shape of aneurysms, which can be accurately reconstructed from anatomic images.

Image-based modeling developments began in the 1990 (Moore *et al.* 1999). Since that time, researchers have used idealized aneurysm geometries or approximations of a patient geometry. Recent advances in computational power, medical imaging and computerized image processing have made possible to reconstruct an accurate 3D representation geometric for a specific patient (Steinman 2002). Consequently, many groups have developed and used these techniques to investigate the pathogenesis of aneurismal disease (Hoi *et al.* 2004) and to calculate rupture risk of these lesion (Hassan *et al.* 2005; Utter and Rossmann 2007). In Addition, they have used computational fluid dynamic (CFD) techniques with very promising results (Cebal *et al.* 2005; Cebal *et al.* 2005; Cebal *et al.* 2007).

Three-dimensional modeling from images for computational analysis in general requires three fundamental steps: image segmentation, model pre-processing and mesh generation. Although, the individual components of the chain could change, the essential steps are conserved. To create a geometric model from images, requires user interaction and can be time-consuming and impractical for large-scale projects. This process depends on the quality of the anatomic images, the complexity of the vascular geometry including the aneurysm and the level of expertise of the modeler (Cebal *et al.* 2005).

Problems related to the segmentation of the vascular tree for the creation of analytic or discrete geometric models are aim of diverse studies (Hernandez *et al.* 2003; Manniesing *et al.* 2008). Three competing approaches have been utilized to create computational models. The first approach is based on segmentation of the lumen boundary in a two-dimensional image. Another approach is the segmentation directly of three-dimensional images. Finally, an intermediate approach is fitting a template geometries to image data.

Another open problem in patient-specific geometric modeling is to create models that include the thickness of the vessel wall. While the solution to this will have to await further advances in medical imaging, new image segmentation and geometric modeling techniques will be needed as well. On the other hand, the challenge in computational methods resides in applying to large numbers of patient-specific aneurysm geometries. To overcome the obstacle of laborious and lengthy data processing and calculations, the whole pipeline must be fully optimized with the goal of reducing or eliminating manual intervention. Additionally, mesh generation has to be capable of handling the realistic complex geometries of aneurysms and its connected vessels so that biases can be reduced in the studied populations for statistical analysis.

The process used to extract models need to be robust to ensure accuracy and reliability. A few studies have been dedicated to validate image-based modeling methods and assessing the uncertainty of measurement data and sensitivity of solutions. Validation of image-based modeling methods is particularly challenging because the vessel wall is moving in response to the pulsatile pressure and, until recently, only time-averaged three-dimensional image data have been available. Although there have been some attempts to assess the sensitivity of hemodynamic solutions to image reconstruction techniques, much more work is needed.

The extraction of patient specific vascular models from medical images offers the possibility to extract complete 3D descriptors of morphology, integrating the limited information available from medical images and estimating these non observable parameters using data assimilation techniques.

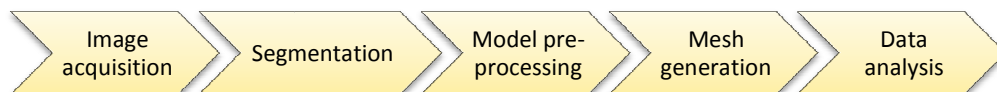


Figure I.7. Standard Image-Based model pipeline

I.5. Morphological Characterization: Literature Overview

Recent literature has focused on comparing anatomical and morphological characteristics of the aneurysms with the goal of explain factors associated with a high risk of rupture. To do an appropriate risk assessment on the rupture of intracranial aneurysms it is indispensable outline the known risk factors. For this purpose, a general overview is given trying to draw and highlight broad inferences, which have tried to improve the clinical management of unruptured intracranial aneurysms.

Author & Date	Study description	Conclusions
Sampei et al. 1991	Examined morphological characteristics of 25 aneurysms.	Found to have grown on repeat angiography and found that the irregular contour and the presence of blebs correlated with faster growth and increased risk of rupture or rebleeding.
ISUIA. Wiebers et al. 1998	The study was divided into 2 cohorts, a retrospective cohort of observed 1937 unruptured aneurysms in 1449 patients, designed to evaluate risk of rupture over time, and a prospective cohort enrolled 1172 patients undergoing treatment, designed to evaluate surgical risk.	In retrospective cohort the risk of rupture for Group 1 for aneurysms < 10 mm in size in the anterior circulation was 0.05% per year, compared with 0.5% annually for Group 2. Aneurysms > 10 mm in size had a risk of rupture close to 1% annually in both groups.
Hademenos et al. 1998	Account of 74 patients with aneurysms (40 ruptured and 34 unruptured) and evaluated the location and morphological factors such as lobulations.	Reported that 16 (84%) of 19 multilobulated aneurysms had ruptured, compared with only 24 (44%) of 55 unilobular aneurysms. Aneurysm morphology and location in the intracranial circulation were statistically significant factors in predicting rupture
Parlea et al. 1999	Characterize the geometry of simple-lobed cerebral aneurysms and to find the absolute size of these lesions from angiographic tracings. Measurements of angiographic neck width (N), dome height (H), dome diameter (D), and semi-axis height (S) were obtained from tracings of 87 simple-lobed lesions. Ratios	For the entire sample, mean ratios were D/H = 1.11, D/N = 1.91, and H/N = 1.86. For the H/S ratio, the value was 1.98 for BB, MCA, and PcomA lesions and significantly smaller for the AcomA subgroup, at 1.52. The average sizes (in mm) for these dimensions were N = 3.4 for MCA, 3.0 for AcomA, 3.1 for PcomA, and 6.5 for BB; D = 6.1 for MCA, 5.9 for AcomA, 5.3 for PcomA, and 11.7 for BB; H = 5.6 for MCA, 5.0 for

	calculated from the simple measurements were analyzed as subgroups according to location	AcomA, 5.3 for PcomA, and 11.3 for BB. On average, BB aneurysms were twice as large as aneurysms at other locations. Good correlations were found between the scaled values for D and N, H and N, and H and D.
Ujje <i>et al.</i> 2001	129 patients with ruptured aneurysms and 72 patients with 78 unruptured aneurysms were evaluated with an index that captures part of the shape from aneurysm namely aspect ratio.	The mean aneurysm size was found to be statistically significant in the aneurysms at the ICA-PComa. However, the mean aspect ratio was statistically significant at all four locations. Almost 80% of ruptured aneurysms had an aspect ratio > 1.6, whereas almost 90% of unruptured aneurysms had an aspect ratio < 1.6.
ISUIA. Wiebers <i>et al.</i> 2003	This report is a follow-up of the previous study in 1998 that evaluated rupture risk based on location and size, and specifically assessed surgical and endovascular treatment risks.	The 5-year cumulative rupture rates for patients without prior SAH, with anterior circulation aneurysms were 0, 2.6, and 14.5% for aneurysms <7, 7–12, and 13–24 mm, respectively, compared with rates of 2.5, 14.5, and 18.4%, for the same size aneurysm in the posterior circulation. Patients with a history of previous SAH with aneurysms < 7 mm in size had a 0.1% yearly rupture rate.
Weir <i>et al.</i> 2003	Examined 774 aneurysms in 532 patients.	Found that the mean aspect ratio of unruptured aneurysms was ~ 1.8 as opposed to 3.4 for ruptured aneurysms. The calculated odds of aneurysm rupture were 20-fold greater when the aspect ratio was > 3.47 as opposed to those < 1.38.
Beck <i>et al.</i> 2003	Detailed 147 aneurysms in 124 patients (94 ruptured and 53 unruptured), examining the presence of lobulations, daughter sacs, and the differences in aneurysm size.	Found that multilobular aneurysms between 5 and 9 mm in dome height were more frequently ruptured than unilobular lesions (26 vs 4%). Furthermore, they could not demonstrate a significant difference based on the presence of a daughter sac, but they had < 10 such lesions in the trial.
Matsubara <i>et al.</i> 2004	Monitored changes in aneurysm morphology in 140 patients with 166 unruptured aneurysms by using serial CT angiography for a	They observed growth or new development of blebs/daughter sacs in 6.4% of patients (6 aneurysms grew and 4 developed blebs). Statistically significant

	mean follow up of 17.7 months. No aneurysm rupture was reported during the duration of the study; however, 7 aneurysms were treated.	predictors were aneurysm size and basilar apex bifurcation or internal carotid artery location. Other predictors of growth were patient or family history of SAH, presence of a preexisting bleb, hyperlipidemia, and diabetes.
Hoi et al. 2004	They used CFD to evaluate the influence of variable arterial curvature on lateral wall aneurysms.	Found that a greater degree of curvature lead to higher degrees of hemodynamic stress, thus possibly increasing rupture risk.
Nader-Sepahi et al. 2004	The study was undertaken to assess the reliability of the aspect ratio in predicting aneurysm rupture. 75 patients with subarachnoid hemorrhage and multiple aneurysms. By comparing the difference between ruptured and unruptured aneurysms in the same individual, each patient in effect served as his or her own control.	There were 75 ruptured and 107 unruptured aneurysms. Found the mean aspect ratio of 2.7 in ruptured aneurysms and 1.8 in unruptured aneurysms. This difference between the ARs was statistically significant ($P < 0.001$). The difference in aneurysm sizes in the two groups also was significant ($P < 0.001$).
Shojima et al. 2004	Evaluated the CFD analyses of 3D CT angiography reconstructions of 20 MCA aneurysms, 3 ruptured and 17 unruptured.	Found, in opposition to most previous reports, that lower WSS, compared with the parent vessel, was present in the dome of aneurysms and in the blebs and/or daughter sacs. In contrast, higher WSS values were found in ruptured aneurysms.
Ma et al. 2004	In this study, quantify the three-dimensional geometry of the aneurysm sac, using computed tomography angiography (CTA) data, the three-dimensional geometry of five unruptured human cerebral aneurysms was reconstructed. The physical meanings of various indices and their possible role as prognosticators for rupture risk and presurgical planning were discussed.	The four hypothetical aneurysms have the same volume, the other 1-D and 2D indices are quite different. This study makes a case for CTA as a better modality than digital subtraction angiography (DSA) in the characterization of brain aneurysm Geometry. The spherical shaped models have lower aspect ratios (AR) than their ellipsoidal shaped counterparts.

-
- Sadatomo et al. 2005** 3DSA was performed in 44 cases of middle cerebral artery aneurysm, 20 unruptured and 24 ruptured. When the neck was located on the extension of the midline of the parent artery, it was defined as Type C; when it was not, it was defined as Type D. Examined 44 aneurysms and reported 19 cases were the mean aspect ratio in ruptured aneurysms was 2.24, significantly greater than 1.56, which was found in unruptured aneurysms. Chi2 test revealed that there were significantly more ruptured cases among Type C (14/19) compared with Type D (10/25).
- Hassan et al. 2005** Examined 68 aneurysms (45 ruptured and 23 unruptured) and classified them into 3 aneurysm groups, namely sidewall, sidewall with a branching vessel, and end wall. Found a 100% rupture rate for aneurysms with an aspect ratio > 1.6 and either a sidewall or sidewall with branching vessel-type, in contrast to 28.75% rate for end wall-type aneurysms. They also found a significantly lower rupture risk and higher flow rates in aneurysms with wide necks and efferent, draining arteries, thus minimizing the inflow.
- Raghavan et al. 2005** They investigated whether quantified shape or size indices could better discriminate between ruptured status by using 3D CTAm models of the brain vasculature. In 27 patients with ruptured or unruptured aneurysms were calculated 5 size and 8 shape indices. None of the five size indices were significantly different between the two lesion groups. 5 of the 8 shape indices were significantly different and two other shape indices showed a trend toward discriminating between ruptured and unruptured aneurysms, although these differences did not reach statistical significance.
- Cebal et al. 2005** Evaluated 62 aneurysm models, based on 3D digital subtraction angiograms from patients, using CFD. These models were divided into 4 types: 1) single inflow jet, single vortex of flow; 2) single inflow jet, multiple vortices; 3) multiple inflow jets, single vortex; and 4) multiple inflow jets, multiple vortices. Type 1 was the most frequently encountered, followed by Type 4, Type 2, and Type 3. Types 4 and 2 were the most frequently multilobulated, large in size, and had a higher aspect ratio. Type 1 aneurysms, in contrast, were more likely to be smaller, unilobular, and have a smaller aspect ratio. The rates of rupture for each type of aneurysm were 27, 45, 60, and 58%, respectively. Still, the only statistically significant predictor of rupture risk in this report was the size of the flow impingement region. Aneurysms with small inflow jet streams or smaller flow impingement size were 6.3 times more likely to have ruptured.
-

Castro et al. 2006	Evaluated 1 posterior communicating artery, 2 middle cerebral artery, and 1 anterior communicating artery by using CFD analysis of WSS.	Found an unequal amount of flow in the carotid arteries could be linked to an asymmetric, increased amount of WSS in the AcomA aneurysm, possibly rendering the aneurysm at a higher rupture risk potential. Included in their study, the effects of parent and draining arteries on CFD analyses, found that not taking into account the inflow of the parent artery as well as outflow through the efferent arteries can significantly underestimate the WSS values in the dome of the aneurysm. When corrected, they found consistently higher values of WSS in the aneurysm domes and blebs.
Sadatomo et al. 2006	Described 18 aneurysms of the Anterior Communicating Artery (ACom), detailing the relationships of the aneurysm to the segment 1(A1), the midline, at the junction of the ACom, and at the A1-A2 junction.	Found that for all patients with codominant A1 segment, the aneurysms were always of the classic type, where the aneurysm fundus arose in the midline, in contrast to patients with a dominant A1, where the aneurysm fundus pointed to the contralateral side of the dominant A1.
Millan et al. 2007	A novel methodology for 3-D shape characterization of cerebral aneurysms is described. The aneurysms are isolated by taking into account a portion of their adjacent vessels. Two methods to characterize their morphology using moment invariants have been considered: geometrical moment invariants (GMI) and Zernike moment invariants (ZMI). The results have been validated in a database containing 53 patients (31 ruptured and 24 unruptured aneurysms).	It has been found that ZMI indices are more robust than GMI, and seem to provide a reliable way to discriminate between ruptured and unruptured aneurysms. Correct rupture prediction rates of approximately equal to 80% were achieved in contrast to 66% that is found when the aspect ratio index is considered.
Hoh et al. 2007	They published aneurysm characteristics of 30 patients with multiple aneurysms, 30 ruptured and 37 unruptured. Seven 1D geometric indices and five 2D indices were evaluated.	Aneurysm height, diameter, aspect ratio, bottleneck factor, and aneurysm/parent artery ratio were all statistically significantly different between unruptured and ruptured aneurysms.

-
- Ahn et al. 2007** Examined in vitro models of 2 intracranial aneurysms to show the feasibility of 3D phase-contrast MRI as an alternative to CFD models. A potential advantage of this technique is the ability to visualize both the rate and inflow hemodynamic. The results showed the highest WSS at the inflow zone of the aneurysms, but they did show a local area in the bleb of one aneurysm and in the dome of the other to have had constant high WSS without temporal variation. These results were consistent with most high WSS theories.
- Juvela et al. 2008** Account of the cumulative aneurysm rupture risk in Finnish patients with long-term follow-up in which 142 patients with 182 aneurysms were evaluated. They found to have a rupture rate of 1.3% per year. They noticed that the majority of ruptured aneurysms were <7 mm and larger aneurysms had a linearly increasing relative risk compared with smaller aneurysms. With respect to aneurysm location, AcomA aneurysms were found to have a higher ratio of ruptured to unruptured aneurysms than other locations.
- Sadatomo et al. 2008** Reported on the relationship among aneurysm neck, parent artery, and daughter branches in 22 consecutive MCA bifurcation aneurysms, which were divided into a classic-type (aneurysm at midline relative to parent artery) and a deviating-type (aneurysm deviates to the side of 1 daughter artery). Found that in all cases, the deviating-type aneurysms were located on the side of the daughter artery with a narrower angle to the parent artery. Furthermore, in > 90% of the cases, the aneurysm was located on the side of the smaller artery, suggesting the dominant artery provided the hemodynamic force for aneurysm formation and likely increased rupture risk; however, this argument could not be shown statistically.
- Dhar et al. 2008** Reported 45 patients (25 ruptured and 20 unruptured terminal or sidewall aneurysms). 8 parameters were calculated (5 old and 3 novels). The old were aspect ratio, aneurysm size, ellipticity, non-sphericity and te></EndNote>Dhar et al. he novel, which incorporated the parent vessel geometry, were vessel, aneurysm angle and aneurysm-to-vessel size ratio. Size ratio and aneurysm angle with respect to the parent artery had the strongest correlation to rupture potential. Although statistically significant differences were also found for aspect ratio, undulation, ellipticity, and non.sphericity index. The fact that these novel parameters involve the aneurysm's relationship to the parent vessel further supports the influence of hemodynamics from the surrounding vasculature on the behavior of the aneurysm.
-

- Meckel et al. 2008** Examined cardiac-gated 3D phase-contrast MR imaging of 5 aneurysms in vivo Found that the highest aspect ratio (2.2) had a single inflow jet with multiple vortices. Two small, smooth aneurysms with the smallest aspect ratios (1.1 and 1.3) had single inflow jets and single vortices. Despite the fact that the WSS was underestimated due to the lack of inflow and outflow boundary corrections, this study showed that in-vivo phase-contrast MRI could correlate flow dynamics, aspect ratio, and fundus size in aneurysms.
- Baumann et al. 2008** Examined only patients with multiple aneurysms, the vast majority of patients had 1 ruptured aneurysm, and the remainder were unruptured. 99 Patient, 90% with SAH and 10% incidental aneurysms. The female to male ratio was 3:1, median age was 53 years. There were 265 aneurysms (median number per patient, 2; range, 2–8), 95% were small (≤ 10 mm), 4.5% large, 0.5% giant (> 25 mm); 34% were ruptured, 66% unruptured (median size, 7mm vs. 4mm; $p < 0.0001$). Most aneurysms (27%) were on the MCA bifurcation. Most ruptured aneurysms (18%) were on the AcomA and were 10mm or smaller.
- Burns et al. 2009** Monitored changes in aneurysm morphology in 165 patients with 191 unruptured aneurysms by using serial MR angiography for a mean follow up of 47 months. A significant limitation of this study was that a large number of patients were lost to follow-up, and growth and rupture rates remained unknown for these patients. They noted that 10% of patients had aneurysm growth over that time period, during which they documented 1 incident of aneurysm rupture. The only statistically significant predictor of growth was previous aneurysm size. For aneurysms < 8 , between 8 and 12, and ≥ 13 mm, the frequency of enlargement was 6.9, 25, and 83%, respectively.
-

I.6. Objectives

As mentioned in the previous section, morphology and haemodynamics are two widely accepted factors as playing an important role in assessing the risk of rupture of cerebral aneurysms. The Middle Cerebral Artery (MCA) is one of the three major paired intracranial arteries and is the largest branch of the Internal Carotid Artery which supplies blood to an important portion of the brain. Aneurysm incidence at this location rises up to the 20% (Brisman et al. 2006) and therefore they are the second most frequent location for intracranial aneurysms. MCA aneurysm incidence is only behind the aneurysms in the Anterior Communicating Artery (30%), but pose less difficulties for obtaining high quality images. Their high incidence and readily availability of images make them suitable candidates to derive clinical conclusions from this population using image-based techniques.

Obtaining hemodynamic simulations from medical images is known to be a time-consuming task because it requires not only the manual intervention of highly-skilled users, but also high computational resources. Morphology is known to be one of the most relevant factors determining the hemodynamic, and under certain circumstances it could be considered as a potential surrogate of hemodynamic. In our case, instead of using Computational Fluid Dynamics techniques, we propose as an alternative the use of several methods (Ma et al. 2004; Raghavan et al. 2005; Millan et al. 2007) to compute accurately and in real-time a number of meaningful parameters describing the cerebral aneurysm morphology, and use them to assess their risk of rupture.

Summarizing, the main objectives of the present study are:

- To prove the feasibility of using a complete and efficient image-based pipeline producing patient-specific models from medical images of patients with a cerebral aneurysm.
- To use these geometric models to obtain a set of representative indices able to efficiently discriminate between ruptured and unruptured aneurysms using statistical tools.
- To provide a morphology-based methodology to support clinical decisions, facilitating patient-specific treatment selection.

To accomplish these objectives, the study has been carried out on a population of MCA aneurysms, but it could be extended to other locations.

Chapter II Materials and Methods

II.1. Patient Population

For each patient information of their age, sex, treatment knows as a patient related risk factors. A total of 79 patients with 95 aneurysms were selected from three clinical centers. Unruptured aneurysms were found in 64 cases, just ruptured aneurysm in 22 cases and in 9 aneurysms the rupture information was not known. Of the entire population, 16 patients present multiple aneurysms. Only lesions located in the Middle Cerebral Artery (MCA) is taken into account, even if the patient had several aneurysms in other intracranial arteries. Patients with not saccular aneurysms, like fusiform, mycotic, or aneurysms involving lenticulostriate branches or distal were excluded of this study. In cases where clinical information was inconclusive or not available, the aneurysms were classified as unknown.

II.2. Reconstructed Models

Diagnostic images were acquired via three-dimensional rotational angiography (3DRA) and were obtained from patients from three different hospitals. The first one, the Department of Radiology of the Foundation of Rothschild, Paris, France (76 aneurysms), used an Integris Allura Neuro (Philips Healthcare, Best, The Netherlands). The second center was NeuroAngiografía Terapéutica (located at the Hospital General de Catalunya), Sant Cugat Del Vallés, Spain (8 cases), using a System Integris Allura Neuro (Philips Healthcare, Best, The Netherlands). The third one was Hospital Clinic i Provincial de Barcelona, Barcelona, Spain (11 aneurysms), acquired using an AXIOM Artis (Siemens Medical Solutions, Erlangen, Germany).

Starting from a medical image and with a database including patient's clinical history the data processing pipeline proposed create patient-specific anatomic models, which are used to derive robust and reliable quantitative descriptors, which will be linked with aneurysm growth or rupture and for patient-specific assessment and treatment planning. The methodologies described here have been developed within the European project @neurIST with an in-house software called AneuFuse, which integrates all operations needed to extract patient-specific vascular models. The program is based on the open-source Visualization Tool Kit (VTK) libraries.

The pipeline describing the steps from medical image to data analysis involves the integration of multiple techniques:

II.2.1. Image Data

Patients were scanned using a 3DRA imaging suite. Angiographic images visualize vessels by suppressing background signal and enhancing the signal corresponding to the vascular lumen. Then, the data is a three dimensional reconstructed as a regular grid of voxels, each with a certain intensity value. In order to increase the intensity of the vasculature, a contrast medium is used. Better visualization and quantification of vascular dimensions are achieved when the transition between luminal intensity and background is sharp. Because 3D data reconstructed from rotational angiographic images (instead of two-dimensional images) were used in this study, we could only include cases in which the images were of sufficiently quality for accurate segmentation and reconstruction.

II.2.2. Image segmentation

Probably the most critical step in vascular modeling, on which most other steps are dependent, is obtaining a proper anatomical representation from the medical images using image segmentation techniques. In this work, an in-house automatic multimodal vessel segmentation algorithm namely Geodesic Active Regions (GAR) implemented and introduced by Hernandez and Frangi 2007, was used to reconstruct vascular models in an automatic manner. This technique has been mainly developed for CT images and has been slightly modified for processing 3DRA and MRA modalities. A combination of geometric deformable models, knowledge-based techniques and image intensity standardization ensure the applicability of this methodology to the image modalities typically used in the study of intracranial aneurysms.

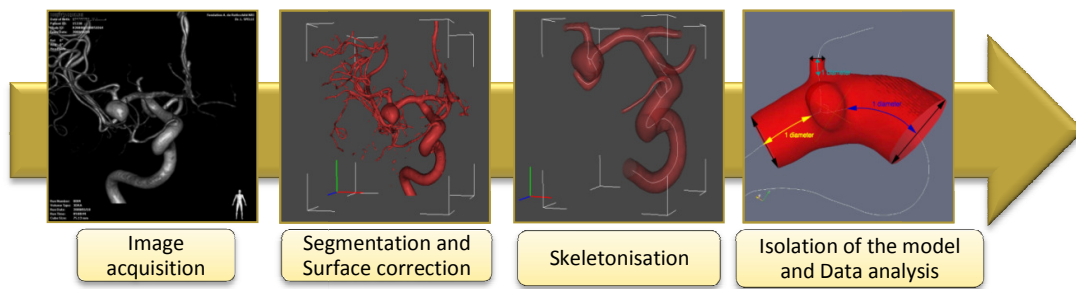


Figure II.1. Data processing pipeline used to obtain the models.

II.2.3. Surface meshing

After segmentation, a three-dimensional computer model is extracted, which is given as a triangulated surface mesh. Artifacts that do not belong to the cerebral vasculature were carefully removed from the reconstructed surface trying to conserve the most reasonable model. The repair process includes a smoothing of the cleaned mesh chosen to minimize shrinking and other errors. This step include manual processing that creates a realistic representation of the relevant part of the intracranial vasculature

II.2.4. Skeleton

A skeleton is a line representation of the 3D domain of the aneurysm and the addition to the surface representation has several advantages. Generally the skeleton supports a more reproducible way to define cutting planes to close the analysis domain. An automatic algorithm integrated in the program to calculate a centerline was used.

II.2.5. Isolation of the model

The neck of the aneurysm was defined as the location from where the aneurismal sac pouched outward from the parent vessel. The centerline helps to perform cuts with planes perpendiculars to the skeleton, in order to obtain a correct isolated model that includes the aneurysm geometry and its surrounding. The criterion for the isolation was defined by using a cutting plane at a distance of approximately one diameter of the parent vessel from the aneurysm neck (See Figure II.2). All further geometric calculations were performed on the isolated aneurysm model, including complete 3D morphological descriptors using custom algorithms.

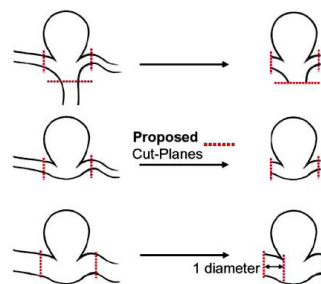


Figure II.2. Proposed cut-planes for isolating aneurysm model, adapted from Millan *et al.* 2007.

II.3. Morphological Characterization

With the computer models of the cerebral vasculature extracted from medical images, it is feasible to analyze the morphology of aneurysms and surrounding vessels in all its complexity. There is much to explore about the potential of this type of analyses to provide better risk assessment on aneurysm rupture. In the literature overview included in Section I.5, some studies proposed multiple shape indices of various complexities. The most relevant ones were chosen and included into our study.

II.3.1. Size indices

These measures are simple in definition and have a clear physical meaning. Two one dimensional size indices were defined: neck width and aneurysm depth. Neck width is the maxima diameter of the curve in the point of is considered the beginning of the aneurysm. Aneurysm depth is the maximal perpendicular distance between the top of the aneurysm dome and the plane of the surface of the neck. With the determination of the neck width and the aneurysm depth values is feasible to calculate the aneurysm volume, the aneurysm area, and the neck area.

II.3.2. Shape indices

Two 2D shape indices were derived based on the 1D size measures: Aspect Ratio (AR) and Non-Sphericity Index (NSI) (See Table II.1).

Ujiie *et al.* 1999 proposed to capture part of the shape of an aneurysm in a single parameter namely Aspect Ratio (AR), based on the hypothesis that flow low flow occurs in aneurysms with a relatively large depth in relation to the aneurysm opening. This geometric index might better describe the aneurysm than just the size. It is calculated with the maximum distance from the neck to the dome divided by the width of the neck (See Figure II.3). Although this parameter has been successfully used to single out small aneurysms with an associated high rupture risk, whereas other studies have shown that it does not always provide accurate predictions (Weir *et al.* 2003).

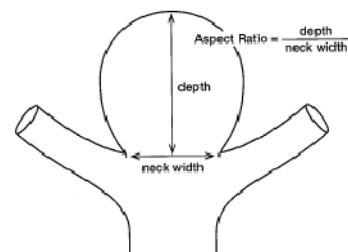
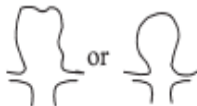


Figure II.3. Graphical definition of the Aspect Ratio, adapted from Ujiie *et al.* 2001.

Non-Sphericity Index (NSI) is an index that calculates the deviation from spherical shape capturing the complete 3D aneurysm geometry. If the wall tension is homogeneously distributed, it is likely to result in a stable lesion with a low risk of rupture, then a spherical shape is likely to be the most stable (Raghavan et al. 2005). The level to which an aneurysm surface deviates from a spherical shape therefore could be a good index of instability. This deviation could come from undulations and/or ellipticity, but both will result in a relative increase in surface area of the lesion compared with its volume. For all practical purposes, NSI will vary from 0 to 1. It is equal to 0 for a hemisphere and increases with increasing deviation from the spherical shape, be it due to undulation or ellipticity.

Table II.1. Schematic and definition of selected shape indices.

	Formula	Low	Medium	High
Aspect Ratio	$\frac{\text{Depth}}{\text{Neck width}}$			
Non-Sphericity Index	$1 - (18\pi)^{1/3}(V/S)^{2/3}$		 or 	 or 

The computation of the shape coefficients used in the morphological characterization are introduced by Millan et al. 2007 and uses Zernike moments (ZM) as shape descriptors. The proposed methodology includes in the shape description the aneurysm dome together with a part of the adjacent vessels. This allows the incorporation in the shape description of some features directly related to hemodynamic inside the aneurysm. For that reason, these indices are used to characterize mathematically in a complete manner the whole geometry.

This mathematical method presents useful properties including translation, scale and rotation invariance. The characterization reduces the geometry of the aneurysm to a limited set of descriptors that represent the shape in a condensed way. Two variants of the Zernike Moments can be computed for a given shape: volume-based and surface-based moments. Surface moments are expected to be better descriptors, since they can distinguish opened extremities from closed terminations (dome or bleb). For the aneurysm and parent vessel, the invariant moments up to order $n=20$, which amounts to 121 descriptors. For the dome only, the moment rise to order $n=10$, which amounts to 24 descriptors. The order ascends up to 20 because this represents a good compromise between computational time and accuracy in the shape description (See Figure II.4.a.).

Millan *et al.* 2005 studied a possible correlation between the morphology and the risk of rupture of aneurysms. They created 3D computer models of aneurysms and portions of their adjacent vessels from patient-specific images on which surface segmentation was performed. Then, the Zernike moments invariant (ZMI) of the models was mathematically characterized. The returned indices placed them in a multi-dimensional space in which models of ruptured aneurysms tended to cluster (See Figure II.4.b.).

Major benefits of this method are to use the full potential of three dimensional information for the morphological characterization of the aneurysm, and it is robust to the small perturbations in the models due to their properties of invariance.

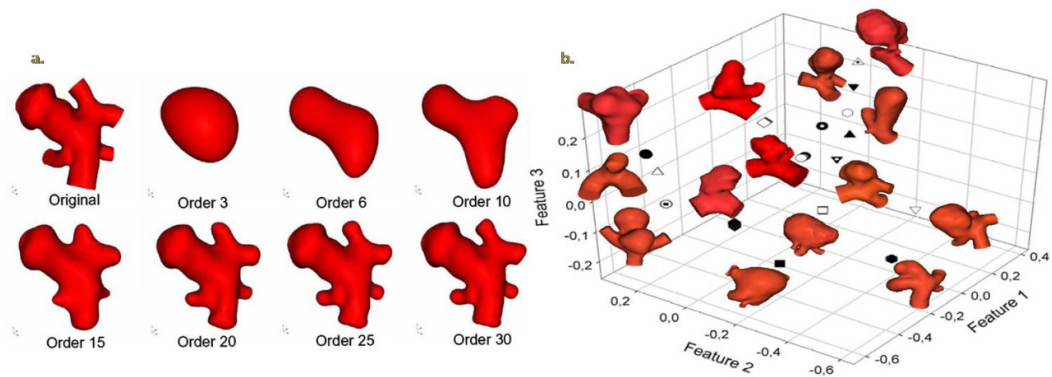


Figure II.4. a) The original volume of the aneurysm in the upper left corner is reconstructed using Zernike moments invariants with different orders. b) 3D representation of the multi-dimensional feature space where the aneurysm is located after retrieving characteristic indices.

II.4. Statistical analysis

Statistical analyses were performed using a software package (SPSS Inc v18.0, IBM Company Headquarters, Chicago, Illinois). Ruptured and unruptured aneurysm groups were analyzed separately. Results were expressed as the mean value and standard deviation of all variables. Aneurysm rupture risk was statistically tested for all parameters. The statistical significance level was set to 0.05. The relationship between The categorical (nominal or ordinal) variables were examined using cross tabulation table. When we have measured only qualitative variables, we analyze frequencies performing the Pearson Chi-square test. This test measures the discrepancy between the observed cell counts, and what you would expect if the variables were unrelated.

First the data were explored prior to any analysis. This allows identifying potential errors and outliers, strange data and unexpected variability, as well as studying with greater precision the form and other characteristics of the distribution patterns. For the distribution, the normality test, namely Kolmogorov-Smirnov, gives a critical level to decide if the population comes from a normal distribution (> 0.05). For variance, the Levene's robust test shows homogeneity of variance (< 0.05). For linearity, the Durbin Watson test verifies if the variables are independent. It is important to confirm these assumptions before deciding which statistical test is the most suitable.

Then, non-parametric tests were performed because they make minimal assumptions about the underlying distribution of the data. Independent-samples non-parametric tests identify differences between two or more groups. The Mann-Whitney test serves to compare two conditions when different participants take part in each condition. This test is the non-parametric equivalent of the independent t-test. The parameters found to be significant in the non-parametric test were further analyzed using linear discriminant analysis, principal component analysis (PCA) and receiver operating characteristics (ROC) to identify the parameters that retained significance when only we take into account relevant variables.

II.4.1. Linear Discriminant Analysis (LDA)

Discriminant analysis builds a predictive model for group membership. The model is composed of a discriminant function based on linear combinations of the predictor variables that provide the best discrimination between the groups. The functions are generated from a sample of cases for which group membership is known and then applied to new cases that have measurements for the predictor variables but with unknown group membership. Once obtained the discriminant function, it can be used to perform a classification of the same cases used to obtain the function. This will provide a first verification of the degree of efficiency of the function from the point of view of the classification. Second, if the results are satisfactory, it will be possible to use the discriminant function for classification of future cases. From these cases only their punctuation in the independent variables is known, and not the group to which they belong. In this case, two strategies are available, the leave-one-out classification or have a larger random sample for the validation. From the original data a random sample is chosen for the validation and the discriminant function is estimated by the remaining cases or sample for training, then the function is used to classify the cases of the sample of validation.

Furthermore, you can select how prior probabilities are determined: if the sizes of the groups are identical then their probabilities are equal. However, if you have an unbalanced design then it is beneficial to base prior probabilities on the observed group sizes.

Two options are available to determine how the independent variables can enter into the model using two different strategies. In the first one, all variables included in the analysis are put together if they satisfy the tolerance criteria. The second one consists of entering the dependent variables using incorporation for steps or stepwise manner. Following this strategy, the variables are joining to the discriminant function one by one and, hereby, it is possible, on the one hand, to construct a function using only those variables that really are useful for the classification and, for the other one, to evaluate the individual contribution of every variable to the discriminant model.

II.4.2. Principal Components Analysis (PCA)

Principal Components Analysis is a method to extract factors to form uncorrelated linear combinations of the observed variables. The first component has the maximum variance. Successive components explain progressively smaller portions of the variance and are all uncorrelated with each other. Principal components analysis is used to obtain the initial factor solution and it can be used when a correlation matrix is singular.

II.4.3. Receiver Operating Curves (ROC)

The Receiver Operating Characteristic (ROC) Curves analysis was also performed for all the indices to quantify the predictability capability for each index. The area under the curve (AUC) values for each parameter were calculated and compared. A larger AUC implies higher sensitivity and higher specificity for that parameter to discriminate between the subgroups. When sensitivity and specificity are plotted, an index with zero predictive capability will be a straight line from the bottom left to top right and the expected curve will be ideally above the diagonal that represents the null hypothesis.

Chapter III Results

The whole set of variables representing the morphology were statistically examined. A total of 79 patients with 95 aneurysms were selected for the study. In total, 64 cases presented unruptured aneurysms, 22 presented ruptured aneurysms and for the 9 cases remaining, the rupture information was unknown.

The patient-related variables are presented in Table III.1. There were 65 female and 20 male patients, where women represent 76.4% of population. The age for ruptured aneurysm is greater than the unruptured group. We found more cases on the left side of the brain vasculature than in the right side.

Table III.1. Patient related variables for unruptured and ruptured aneurysms.

		Unruptured (%),(mean±SD)	Ruptured (%),(mean±SD)
Sex	Male	14 (16.5%)	6 (7.1%)
	Female	49 (57.6%)	16 (18.8%)
Side	Left	34 (35.8%)	8 (8.4%)
	Right	30 (31.6%)	14 (14.7%)
Age		54.5±10.5	55.8±13.9

For examining the relationship between categorical variables, we analyze frequencies performing the Pearson Chi-square test. From the test, we concluded that there was not a significant association between the gender and the side with the rupture status. Regarding the age, the most common age range for unruptured and ruptured groups was the 61-70 and 51-60 year-old category respectively (See Figure III.1). Moreover, we did not find significant differences between age and the rupture.

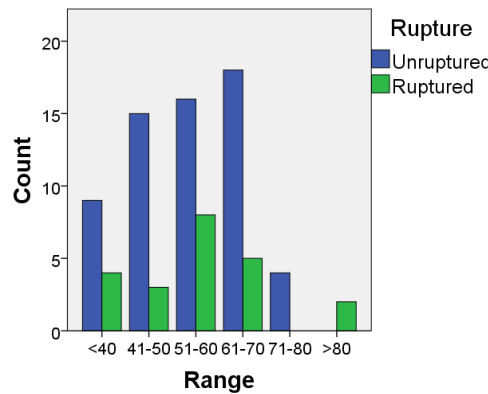


Figure III.1. Bar graphs showing patient's age distribution of the population.

For each isolated model, indices described in the previous section I.5, were divided into two classes according to the measurements location: the dome alone and the dome with a portion of the adjacent vessels. The geometrical variables are only measured for the dome; instead the Zernike moments are calculated for the two location classes. Each of one contains the two ways, surface-like and volume-like (See Table III.3).

Furthermore, we verify if the data obey some assumptions like normal distribution, homogeneity of variance and linearity. The major part of variables did not pass assumptions, for that reason we decide to use nonparametric test. Those tests are less restrictive because they make fewer assumptions about the type of data on which they can be used.

Table III.2 presents the comparison of geometrical indices (size and shape) between the two lesions groups. We have found differences statistically significant between the rupture status in the aneurysm depth, aspect ratio, aneurysm volume, aneurysm area and non-sphericity index ($p < 0.05$). Regarding the aspect ratio, for ruptured aneurysms we found a smaller threshold than reported in the literature (1.38 instead of 1.6, Ujiie et al. 1999).

Table III.2. Size and shape indices for unruptured and ruptured aneurysms.

Index	Unruptured (mean ±SD)	Ruptured (mean ±SD)	p value	AUC
Neck Width	4.22±1.52	4.77±1.68	ns	ns
Neck Area	11.15±7.01	13.98±8.91	ns	ns
Aneurysm Depth	4.69±3.40	6.04±2.54	0.010	0.685
Aspect Ratio	1.05±.46	1.38±.77	0.038	0.649
Aneurysm Volume	96.49±170.23	158.10±213.52	0.016	0.673
Aneurysm Area	79.95±90.20	123.05±104.86	0.013	0.678
Non-Sphericity Index	0.13±.07	0.1808±0.06	0.010	0.685

Figure III.2 displays the box plots for the three principal indices remarking differences between the lesions groups.

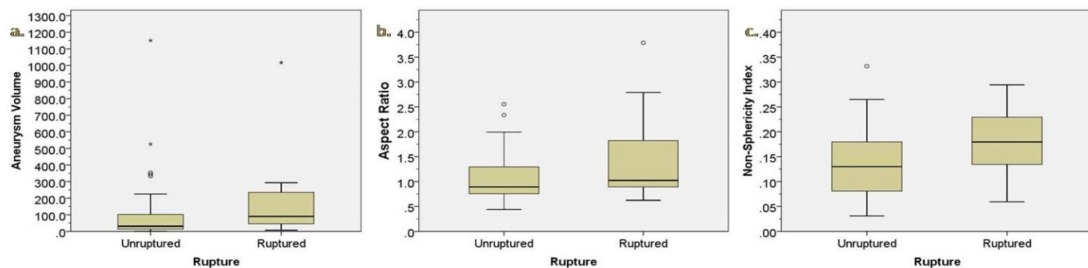


Figure III.2. Box plots of the common studied indices that showed difference statistical significance between the groups. Circles symbols are the outliers.

It is worth to mention that the Zernike moments for the dome provide 36 shape features for each isolated model, whereas Zernike moments for the dome and the parent vessel provide 121 when moments up to order 20 are used. For Zernike moments, small percentages of all set of variables were found to be statistically significant ($p < 0.05$) (See Table III.3).

Table III.3. Indices grouped according to where the measures were obtained and their significance.

	Dome			Dome and parent vessel	
	Geometrical	ZM volume-like	ZM surface-like	ZM volume-like	ZM surface-like
Number of variables	7	36	36	121	121
Number of variables statistically significant	5 (71.4%)	3 (8.3%)	6 (16.7%)	34 (28.1%)	4 (3.3%)

The subgroups of the variables statistically significant were then introduced to a discriminant analysis. In this analysis, we choose both prior probabilities based on the size or on equal within the groups. In addition, we did the step-wise method. These methods were performed with the strategy of leave-one-out classification. Also, we perform a strategy for classification in a couple of variables with a 50% of random samples for training and the other half to obtain the validation.

Table III.4 shows the percentage of original grouped cases and the cross-validation of the cases correctly classified for all set of variables. The probability was taken into 2 strategies: based on the size of the groups, and equal within the groups.

Table III.4. Indices evaluated as rupture predictors using discriminant analysis.

		Dome			Dome and parent vessel	
		Geometrical	ZM volume-like	ZM surface-like	ZM volume-like	ZM surface-like
Probability based on size	Original grouped cases (%)	77.9	74.4	74.4	84.9	74.4
	Cross-validated grouped cases correctly classified (%)	69.8	73.3	70.9	70.9	72.1
Probability equal	Original grouped cases (%)	66.3	69.8	61.6	81.4	69.8
	Cross-validated grouped cases correctly classified (%)	61.6	66.3	54.7	66.3	65.1

The Table III.5 summarizes the step-wise method with the number of significant variables that enter to the model, the percentage of original grouped cases and the cross-validation of the cases correctly classified for all set of variables. A total of seven parameters resulted significant and entered to the analysis.

Table III.5. Step-wise method to enter variables into the model for the discriminant analysis.

	Dome			Dome and parent vessel	
	Geometrical	ZM volume-like	ZM surface-like	ZM volume-like	ZM surface-like
Number of variables enter to de model	1/5 (non-sphericity index)	2/3 ([1,1] [6,6])	2/3 ([2,0] [4,4])	2/34 ([3,1] [14,0])	0/4
Original grouped cases (%)	75.6	74.4	76.7	82.6	Na
Cross-validation (%)	73.3	74.4	75.6	77.9	na

With a 50% of the random sample the model was trained and the validation was done with the lacking cases. Table III.6 shows the rate of accuracy in the training sample and in the respective validation. Therefore, these rates show the accuracy of the discriminant function to classify future cases.

Table III.6. Random sample for training and for validation.

		Selected original grouped cases correctly classified or training sample (%)	Unselected original grouped cases correctly classified or validation sample(%)
Dome Dome and parent vessel	Geometrical	73.9	80
	ZM volume-like	95.7	47.5

A principal component analysis (PCA) had been performed to reduce the dimensionality of the data and to estimate linear components and how a particular variable might contribute to that component. Regarding the Table III.7, it has been found that a few components, typically between 1 and 5, accounted for a high percentage of the variance in the original feature space. The ruptured cluster in each subgroup of variables explains a higher value of variance and extracted components.

Table III.7. Principal component analysis performed in the significant variables. R and U stand for ruptured and unruptured, respectively.

	Dome						Dome and parent vessel			
	Geometrical		ZM volume-like		ZM surface- like		ZM volume-like		ZM surface- like	
	R	U	R	U	R	U	R	U	R	U
Extracted components	2	1	2	1	3	1	5	5	2	1
Explained variance (%)	94.2	75.9	93.5	61.6	94.9	89.1	91.7	90.1	72.9	64.4

We calculated the ROC-AUC for all indices. The AUC for all geometrical indices is also listed in Table III.2. The ROC curves for selected size and shape indices are shown in Figure III.3. The curves are subgrouped following the Table III.3. Regarding the ROC plot for geometrical variables (See Figure III.3.a.), all curves were above the null predictor and the AUC shows a higher value to the non-sphericity index followed by aneurysm depth, aneurysm area, aneurysm volume and aspect ratio. For the Zernike moments plots (See Figure III.3.b.,c.,d.,e.), some indices of each subgroup were slightly below the reference line that represents a predictive capability.

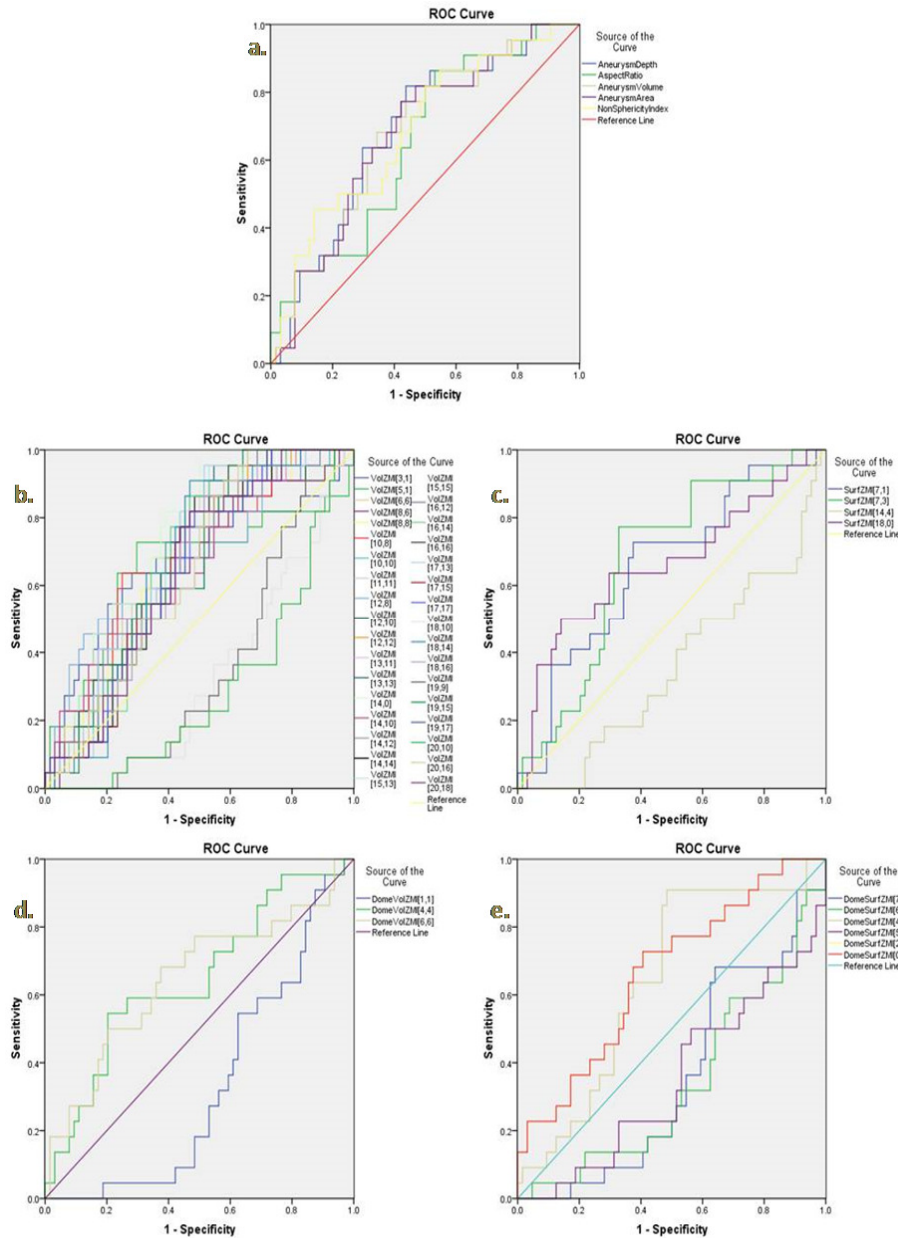


Figure III.3. A Receiver operating characteristics (ROC) curves for all parameters subdivided according to the Table III.3.

Chapter IV Discussion and Limitations

The correlation between rupture risk and morphological parameters describing an aneurysm, has been investigated in this study. Moreover, the capability of the Zernike moment invariants as reliable rupture risk predictors has been analyzed. In addition to previously proposed parameters, we include parameters that also incorporate the parent vessel geometry. We strongly believe that aneurysm shape could be an extremely important factor and identifying reliable indicators of risk for rupture of a lesion could significantly improve clinical management of intracranial aneurysms.

Geometric variables such as the aspect ratio, volume and non-sphericity index are correlated to the aneurysm rupture event for higher aspect ratio, higher non-sphericity index and larger aneurysm volume. The group of ruptured aneurysms have larger mean values than the group of unruptured. Between aspect ratio vs. volume and aspect ratio vs. non-sphericity index, a weak correlation was found and their combination does not seem to be able to classify between the ruptured and unruptured classes.

Aspect ratio for ruptured aneurysms was found to present a smaller threshold than reported in the literature. A possible explanation for this behavior is that in our study aspect ratio was automatically computed from the 3D reconstructed model, while in the literature it was measured from the 2D projection views. For this reason, a common technical limitation in the previous studies on cerebral aneurysm is the use of 2D angiographic data for defining and calculating shape features. Measurement of geometric features can vary with the projection used, resulting in multiple findings for the same aneurysm due to its inherent asymmetrical structure (Black *et al.* 1988).

Inherent limitations exist in any attempt to study factors of aneurysm rupture risk. Unfortunately, this methodology does not account for the possible changes in morphology and other factors such as hemodynamic that unruptured aneurysms may experience over time. Examining a population over time without treatment is desirable but due to the unacceptable ethical dilemma present with regard to patient safety such a study will never be completed. For that reason, studies like the one proposed, are important because they use image-based modeling to elucidate possible factors involved in the risk. On the one hand, in this work a single aneurysm location was selected (MCA) which presents an aneurysm incidence of 20%. Nevertheless, in the literature it has been reported

that other aneurysm's location present higher frequencies of rupture. On the other hand, the current ratio is 22 ruptured vs. 62 unruptured suggests that a larger number of ruptured aneurysms could be included in further studies.

The results obtained after using discriminant analysis were more accurate when choosing prior probabilities based on the size of the groups. The higher percentage seems to be for the volume-based ZM applied to the whole geometry. In addition, when the step-wise method was used the accuracy in the cross-validation increased in comparison with the previous analyses. With this method only a part of the variables had a higher weight and could be included into the model. In the case of geometrical variables, the only significant variable was the non-sphericity index. For the originally group of 400 variables, a set of only 7 variables were finally part of the discriminant function. For the training strategy, we found in the geometrical variables an elevated percentage in the selected cases and in the unselected grouped cases correctly. Instead, in the volume-like of Zernike moments, we found a high percentage in the originally cases but not a sufficient good percentage in the unselected group for validation. Ideally, if the two percentages are properly high the discriminate function can be used for the classification of further cases. A further validation of these results is needed requiring a major number of repetitions to see if the achieved percentages are maintained. Summarizing for the dome surface-based moments, they consistently show better results than the volume-based moments, whereas for the dome with the parent vessel, the result was totally the opposite.

In the case of the PCA analysis, the matrix of components can be explained in the case of the geometrical variables. For the unruptured case, all the variables saturate in a unique factor. For the rupture case, the first component presents high correlation values for the aneurysm depth, volume and area; and for the second component the other variables are explained. Here, it seems that the first component makes reference to the simpler 1D measurements and in the second component to the shape of the aneurysm. In the case of ZM it is hard to explain why the variables are divided into these components because there is not a direct physical meaning of the individual indices.

Among the geometrical variables, we found that the non-sphericity index presented a tendency to have a higher prediction capability followed by aneurysm depth, aneurysm area, aneurysm volume and aspect ratio, in this order.

Chapter V Conclusions and Further work

Morphology has been considered as a potential surrogate of rupture. In this project, morphological variables characterizing cerebral aneurysms have been studied. We have proved the feasibility of using a complete and efficient image-based pipeline producing patient-specific models from medical images of patients with a cerebral aneurysm. We have used these geometric models of the aneurysm sac including the parent vessel to obtain a set of representative indices. Among the set of proposed indices, statistical studies show that the more tridimensional information the morphological descriptors contain, the more robust they are discriminating between ruptured and unruptured aneurysms. This is the case for volume-based Zernike moments, which provided the best prediction results compared to other descriptors such as the Non-Sphericity Index.

This kind of studies should be further validated considering other locations, including more ruptured cases and performing fluid simulations as well. As a result, links should be established with the morphological descriptors proposed in this work. Furthermore, known clinical risk factors like age, sex, smoking habits and hypertension are also fundamental to elucidate the influence of variables chosen when assessing the risk of rupture. These should provide a more comprehensive methodology that would allow supporting clinical decisions, facilitating patient-specific treatment selection.

Each aneurysm is a unique combination of geometry, size, location and relationship with its surrounding vasculature. It is not unreasonable to think that the risk of aneurysm rupture will be determined by a multitude of factors that also include genetics, other diseases present, familial history and patient's age. Definitely the parameters proposed in this work do not suffice on their own to explain the natural history of an aneurysm leading to rupture. Naturally, future research will need to carefully weight all these factors.

Acknowledgements

First of all, I gratefully acknowledge the invaluable collaboration of my daily supervisor Mari Cruz Villa Uriol, who has guided me during the whole year to achieve and well focus my project. I also would like to thank Dr Carles Falcon Falcon for being the director of my project and for the huge support for the discussion part as well to Beatriz F. Giraldo Giraldo for the enormous help in statistics. The high level of collaboration and share of information have made this project possible.

Furthermore, I would like to thank the economical support provided by the European Commission and more specifically to the @neurIST project. A special thanks to Alejandro Frangi for offering me the opportunity to work in the Computational Imaging and Simulation Technologies in Biomedicine group (CISTIB) in Barcelona. Finally, I thankfully appreciate the several contributions provided by different people in the lab such as Minsuok Kim, Jose María Pozo and Hernán Morales.

List of figures

Figure I.1. Schematic representation of the Circle of Willis at the base of the brain. Taken from Rhcastilhos 2007.....	12
Figure I.2. Aneurysm appearance. Taken from National Heart 2010.....	13
Figure I.3. Types of aneurysms a. Saccular b. Saccular wide neck c. Fusiform d. Mycotic; Adapted from Eymann 2004.	14
Figure I.4. Frequent Locations and Incidence of Intracranial aneurysms. Taken from Brisman et al. 2006.	15
Figure I.5. Current treatments available for intracranial aneurysms. a. Clipping. b. Coiling. c. Stent-assisted coiling. Adapted from Brisman et al. 2006.	17
Figure I.6. Different image acquisition modalities a), b) and c) CTA, MRA and 3DRA equipments d), e) and f) different images from the respective modality. Adapted from Radiological Society of North America 2008.....	19
Figure I.7. Standard Image-Based model pipeline.....	21
Figure II.1. Data processing pipeline used to obtain the models.	31
Figure II.2. Proposed cut-planes for isolating aneurysm model, adapted from Millan <i>et al.</i> 2007.....	32
Figure II.3. Graphical definition of the Aspect Ratio, adapted from Ujiie <i>et al.</i> 2001.	33
Figure II.4. a) The original volume of the aneurysm in the upper left corner is reconstructed using Zernike moments invariants with different orders. b) 3D representation of the multi-dimensional feature space where the aneurysm is located after retrieving characteristic indices.	35
Figure III.1. Bar graphs showing patient’s age distribution of the population.....	38
Figure III.2. Box plots of the common studied indices that showed difference statistical significance between the groups. Circles symbols are the outliers.	39
Figure III.3. A Receiver operating characteristics (ROC) curves for all parameters subdivided according to the Table III.3.	42

List of tables

Table II.1. Schematic and definition of selected shape indices.	34
Table III.1. Patient related variables for unruptured and ruptured aneurysms.	38
Table III.2. Size and shape indices for unruptured and ruptured aneurysms.	39
Table III.3. Indices grouped according to where the measures were obtained and their significance.	40
Table III.4. Indices evaluated as rupture predictors using discriminant analysis.	40
Table III.5. Step-wise method to enter variables into the model for the discriminant analysis.	41
Table III.6. Random sample for training and for validation.	41
Table III.7. Principal component analysis performed in the significant variables. R and U stand for ruptured and unruptured, respectively.	41

Bibliography

AHN, S., SHIN, D., et al. *Fluid-induced wall shear stress in anthropomorphic brain aneurysm models: MR phase-contrast study at 3 T*. *J Magn Reson Imaging*. 25 (6), 2007, p. 1120-30.

ANXIONNAT, R., BRACARD, S., et al. *Intracranial aneurysms: clinical value of {3D} digital subtraction angiography in the therapeutic decision and endovascular treatment*. *Radiology*. 218 (3), 2001, p. 799-808.

BAUMANN, F., KHAN, N., et al. *Patient and aneurysm characteristics in multiple intracranial aneurysms*. *Acta Neurochir Suppl*. 103, 2008, p. 19-28.

BECK, J., ROHDE, S., et al. *Difference in configuration of ruptured and unruptured intracranial aneurysms determined by biplanar digital subtraction angiography*. *Acta Neurochir (Wien)*. 145 (10), 2003, p. 861-5; discussion 865.

BLACK, S.P., LEO, H.L., et al. *Recording and measuring the interior features of intracranial aneurysms removed at autopsy: method and initial findings*. *Neurosurgery*. 22 (1 Pt 1), 1988, p. 40-4.

BRISMAN, J.L., SONG, J.K., et al. *Cerebral aneurysms*. *N Engl J Med*. 355 (9), 2006, p. 928-39.

BURNS, J.D., HUSTON, J., 3RD, et al. *Intracranial aneurysm enlargement on serial magnetic resonance angiography: frequency and risk factors*. *Stroke*. 40 (2), 2009, p. 406-11.

CASTRO, M.A., PUTMAN, C.M., et al. *Computational fluid dynamics modeling of intracranial aneurysms: effects of parent artery segmentation on intra-aneurysmal hemodynamics*. *American Journal of Neuroradiology*. 27 (8), 2006, p. 1703-9.

CEBRAL, J.R., CASTRO, M.A., et al. *Characterization of cerebral aneurysms for assessing risk of rupture by using patient-specific computational hemodynamics models*. *American Journal of Neuroradiology*. 26 (10), 2005, p. 2550-9.

CEBRAL, J.R., CASTRO, M.A., et al. (2005). *Pilot clinical study of aneurysm rupture using image-based computational fluid dynamics models*. *SPIE Medical Imaging*.

CEBRAL, J.R., PERGOLIZZI, R.S., JR., et al. *Computational fluid dynamics modeling of intracranial aneurysms: qualitative comparison with cerebral angiography*. *Academic Radiology*. 14 (7), 2007, p. 804-13.

CONNOLLY, E.S., JR. and SOLOMON, R.A. *Management of symptomatic and asymptomatic unruptured aneurysms*. *Neurosurg Clin N Am*. 9 (3), 1998, p. 509-24.

DANDY, W.E. and SCHLESINGER, E.B.D. *Intracranial arterial aneurysms*. Ithaca, N. Y., Comstock Publishing Company.1944.

DHAR, S., TREMMEL, M., et al. *Morphology parameters for intracranial aneurysm rupture risk assessment*. *Neurosurgery*. 63 (2), 2008, p. 185-96; discussion 196-7.

- EYMANN, S. *Flow-assisted aneurysm surgery*, Transonic Systems Inc. 2004.
- FRANCO FOLINO, A. *Cerebral Autoregulation and Syncope. Progress in Cardiovascular Diseases*. 50 (1), 2007, p. 49-80.
- FROSEN, J. (2006). *The Pathobiology of the Saccular Cerebral Artery Aneurysm Rupture and Repair - A Clinicopathological and Experimental Approach*. Department of Neurosurgery and Transplantation Laboratory. Helsinki, University of Helsinki. PhD.
- FROSEN, J., PIIPPO, A., et al. *Remodeling of saccular cerebral artery aneurysm wall is associated with rupture: histological analysis of 24 unruptured and 42 ruptured cases*. *Stroke*. 35 (10), 2004, p. 2287-93.
- GUGLIELMI, G., VINUELA, F., et al. *Electrothrombosis of saccular aneurysms via endovascular approach. Part 1: electrochemical basis, technique, and experimental results*. *Journal of Neurosurgery*. 75 (1), 1991, p. 1-7.
- HADEMENOS, G.J., MASSOUD, T.F., et al. *Anatomical and morphological factors correlating with rupture of intracranial aneurysms in patients referred for endovascular treatment*. *Neuroradiology*. 40 (11), 1998, p. 755-60.
- HASSAN, T., EZURA, M., et al. *Computational simulation of therapeutic parent artery occlusion to treat giant vertebrobasilar aneurysm*. *American Journal of Neuroradiology*. 25 (1), 2004, p. 63-8.
- HASSAN, T., TIMOFEEV, E.V., et al. *A proposed parent vessel geometry-based categorization of saccular intracranial aneurysms: computational flow dynamics analysis of the risk factors for lesion rupture*. *Journal of Neurosurgery*. 103 (4), 2005, p. 662-80.
- HERNANDEZ, M. and FRANGI, A.F. *Non-parametric geodesic active regions: method and evaluation for cerebral aneurysms segmentation in {3DRA} and {CTA}*. *Medical Image Analysis*. 11 (3), 2007, p. 224-41.
- HERNANDEZ, M., FRANGI, A.F., et al. *Three-dimensional segmentation of brain aneurysms in {CTA} using non-parametric region-based information and implicit deformable models: method and evaluation*. *Medical Image Computing and Computer-Assisted Intervention - Miccai 2003, Pt 2*. 2879, 2003, p. 594-602.
- HOH, B.L., SISTROM, C.L., et al. *Bottleneck factor and height-width ratio: association with ruptured aneurysms in patients with multiple cerebral aneurysms*. *Neurosurgery*. 61 (4), 2007, p. 716-22; discussion 722-3.
- HOI, Y., MENG, H., et al. *Effects of arterial geometry on aneurysm growth: three-dimensional computational fluid dynamics study*. *Journal of Neurosurgery*. 101 (4), 2004, p. 676-81.
- HOP, J.W., RINKEL, G.J., et al. *Case-fatality rates and functional outcome after subarachnoid hemorrhage: a systematic review*. *Stroke*. 28 (3), 1997, p. 660-4.
- JOHNSTON, S.C., SELVIN, S., et al. *The burden, trends, and demographics of mortality from subarachnoid hemorrhage*. *Neurology*. 50 (5), 1998, p. 1413-8.

JUVELA, S. *Minor leak before rupture of an intracranial aneurysm and subarachnoid hemorrhage of unknown etiology. Neurosurgery.* 30 (1), 1992, p. 7-11.

JUVELA, S., PORRAS, M., et al. *Natural history of unruptured intracranial aneurysms: probability of and risk factors for aneurysm rupture. J Neurosurg.* 108 (5), 2008, p. 1052-60.

KAYEMBE, K.N., SASAHARA, M., et al. *Cerebral aneurysms and variations in the {Circle} of {Willis}. Stroke.* 15 (5), 1984, p. 846-50.

MA, B., HARBAUGH, R.E., et al. *Three-dimensional geometrical characterization of cerebral aneurysms. Ann Biomed Eng.* 32 (2), 2004, p. 264-73.

MALEK, A.M., ALPER, S.L., et al. *Hemodynamic shear stress and its role in atherosclerosis. JAMA.* 282 (21), 1999, p. 2035-42.

MANNIESING, R., VIERGEVER, M.A., et al. *Cerebral arteries: fully automated segmentation from {CT} angiography: a feasibility study. Radiology.* 247 (3), 2008, p. 841-6.

MATSUBARA, S., HADEISHI, H., et al. *Incidence and risk factors for the growth of unruptured cerebral aneurysms: observation using serial computerized tomography angiography. J Neurosurg.* 101 (6), 2004, p. 908-14.

MCKINNEY, A.M., PALMER, C.S., et al. *Detection of aneurysms by 64-section multidetector {CT} angiography in patients acutely suspected of having an intracranial aneurysm and comparison with digital subtraction and {3D} rotational angiography. American Journal of Neuroradiology.* 29 (3), 2008, p. 594-602.

MECKEL, S., STALDER, A.F., et al. *In vivo visualization and analysis of {3D} hemodynamics in cerebral aneurysms with flow-sensitized {4D} {MR} imaging at 3 {T}. Neuroradiology.* 50 (6), 2008, p. 473-84.

MENGHINI, V.V., BROWN, R.D., JR., et al. *Clinical manifestations and survival rates among patients with saccular intracranial aneurysms: population-based study in Olmsted County, Minnesota, 1965 to 1995. Neurosurgery.* 49 (2), 2001, p. 251-6; discussion 256-8.

MILLAN, R.D., DEMPERS-MARCO, L., et al. *Morphological characterization of intracranial aneurysms using {3D} moment invariants. IEEE Transactions on Medical Imaging.* 26 (9), 2007, p. 1270-82.

MILLAN, R.D., HERNANDEZ, M., et al. (2005). *Characterization of cerebral aneurysms using {3D} moment invariants.* SPIE Medical Imaging.

MOORE, J.A., RUTT, B.K., et al. *Computational blood flow modeling based on in vivo measurements. Ann Biomed Eng.* 27 (5), 1999, p. 627-40.

MOORE, K.L. and DALLEY, A.F. *Clinically oriented anatomy.* Philadelphia, Lippincott Williams & Wilkins.1999.

MORITAKE, K., HAZAMA, F., et al. *Variation of the {Circle} of {Willis} related to the pathogenesis of cerebral aneurysm. Neurologia Medico-Chirurgica.* 16 (5 pt 2), 1976, p. 427-35.

NADER-SEPAHI, A., CASIMIRO, M., et al. *Is aspect ratio a reliable predictor of intracranial aneurysm rupture? Neurosurgery.* 54 (6), 2004, p. 1343-7; discussion 1347-8.

NAKAGAWA, T. and HASHI, K. *The incidence and treatment of asymptomatic, unruptured cerebral aneurysms. J Neurosurg.* 80 (2), 1994, p. 217-23.

NATIONAL HEART, L.A.B.I.N. (2010). "Aneurysms" <http://www.web-books.com/eLibrary/Medicine/Cardiovascular/Aneurysm.htm>, Retrieved 05 January, 2010,

NIEN, Y.L., MURAYAMA, Y., et al. *Endovascular treatment of giant intracranial aneurysms. Neurosurgery.* 51 (2), 2002, p. 547-548.

PARLEA, L., FAHRIG, R., et al. *An analysis of the geometry of saccular intracranial aneurysms. AJNR Am J Neuroradiol.* 20 (6), 1999, p. 1079-89.

PIOTIN, M., SPELLE, L., et al. *Intracranial aneurysms coiling with matrix: immediate results in 152 patients and midterm anatomic follow-up from 115 patients. Stroke.* 40 (1), 2009, p. 321-3.

PIOTIN, M., SPELLE, L., et al. (2007). Intracranial Aneurysms: Treatment with Bare Platinum Coils—Aneurysm Packing, Complex Coils, and Angiographic Recurrence. 243: 500-508.

POETHKE, J., GOUBERGRITS, L., et al. (2008). *Impact of imaging modality for analysis of a cerebral aneurysm: comparison between {CT}, {MRI} and {3DRA}*. Proceedings of European Conference of the International Federation for Medical and Biological Engineering, Antwerp, Belgium, Springer-Verlag Berlin Heidelberg.

RAAYMAKERS, T.W., RINKEL, G.J., et al. *Mortality and morbidity of surgery for unruptured intracranial aneurysms: a meta-analysis. Stroke.* 29 (8), 1998, p. 1531-8.

RADIOLOGICAL SOCIETY OF NORTH AMERICA, I.R. (2008). "Radiology Info" <http://www.radiologyinfo.org> RadiologyInfo, Retrieved 25 January 2010,

RAGHAVAN, M.L., MA, B., et al. *Quantified aneurysm shape and rupture risk. Journal of Neurosurgery.* 102 (2), 2005, p. 355-62.

RAJA, P.V., HUANG, J., et al. *Microsurgical clipping and endovascular coiling of intracranial aneurysms: a critical review of the literature. Neurosurgery.* 62 (6), 2008, p. 1187-202; discussion 1202-3.

RHCASTILHOS. (2007). "Circle of Willis" http://en.wikipedia.org/wiki/File:Circle_of_Willis_en.svg, Retrieved 05 February, 2010,

RINKEL, G.J. *Natural history, epidemiology and screening of unruptured intracranial aneurysms. Journal of Neuroradiology. Journal de Neuroradiologie.* 35 (2), 2008, p. 99-103.

SADATOMO, T., YUKI, K., et al. *Evaluation of relation among aneurysmal neck, parent artery, and daughter arteries in middle cerebral artery aneurysms, by three-dimensional digital subtraction angiography. Neurosurg Rev.* 28 (3), 2005, p. 196-200.

SADATOMO, T., YUKI, K., et al. *The characteristics of the anterior communicating artery aneurysm complex by three-dimensional digital subtraction angiography. Neurosurg Rev.* 29 (3), 2006, p. 201-7.

SADATOMO, T., YUKI, K., et al. *Morphological Differences between Ruptured and Unruptured Cases in Middle Cerebral Artery Aneurysms. Neurosurgery.* 15, 2008, p. 15.

SAMPEI, T., MIZUNO, M., et al. *[Clinical study of growing up aneurysms: report of 25 cases]*. *No Shinkei Geka*. 19 (9), 1991, p. 825-30.

SCHIEVINK, W.I. *Intracranial aneurysms*. *New England Journal of Medicine*. 336 (1), 1997, p. 28-40.

SHOJIMA, M., OSHIMA, M., et al. *Magnitude and role of wall shear stress on cerebral aneurysm: computational fluid dynamic study of 20 middle cerebral artery aneurysms*. *Stroke*. 35 (11), 2004, p. 2500-5.

STEBBENS, W.E. *Aneurysms and Anatomical Variation of Cerebral Arteries*. *Arch Pathol*. 75, 1963, p. 45-64.

STEBBENS, W.E. *Intracranial aneurysms*. *Pathology of the Cerebral Blood Vessels*. St. Louis, MO, Mosby 1972, p. 351-470.

STEINMAN, D.A. *Image-based computational fluid dynamics modeling in realistic arterial geometries*. *Annals of Biomedical Engineering*. 30 (4), 2002, p. 483-97.

UJII, H., TACHIBANA, H., et al. *Effects of size and shape (aspect ratio) on the hemodynamics of saccular aneurysms: a possible index for surgical treatment of intracranial aneurysms*. *Neurosurgery*. 45 (1), 1999, p. 119-29; discussion 129-30.

UJII, H., TAMANO, Y., et al. *Is the aspect ratio a reliable index for predicting the rupture of a saccular aneurysm?* *Neurosurgery*. 48 (3), 2001, p. 495-502; discussion 502-3.

UTTER, B. and ROSSMANN, J.S. *Numerical simulation of saccular aneurysm hemodynamics: influence of morphology on rupture risk*. *Journal of Biomechanics*. 40 (12), 2007, p. 2716-22.

VAN GIJN, J. and RINKEL, G.J. *Subarachnoid haemorrhage: diagnosis, causes and management*. *Brain*. 124 (Pt 2), 2001, p. 249-78.

VANNINEN, R.L., HERNESNIEMI, J.A., et al. *Magnetic resonance angiographic screening for asymptomatic intracranial aneurysms: the problem of false negatives: technical case report*. *Neurosurgery*. 38 (4), 1996, p. 838-40; discussion 840-1.

WEIR, B., AMIDEI, C., et al. *The aspect ratio (dome/neck) of ruptured and unruptured aneurysms*. *Journal of Neurosurgery*. 99 (3), 2003, p. 447-51.

WIEBERS, D.O., WHISNANT, J.P., et al. *Unruptured intracranial aneurysms: risk of rupture and risks of surgical intervention. {International} {Study} of {Unruptured} {Intracranial} {Aneurysms} {Investigators}*. *New England Journal of Medicine*. 339 (24), 1998, p. 1725-33.

WIEBERS, D.O., WHISNANT, J.P., et al. *Unruptured intracranial aneurysms: natural history, clinical outcome, and risks of surgical and endovascular treatment*. *Lancet*. 362 (9378), 2003, p. 103-10.

YANAKA, K., NAGASE, S., et al. *Management of unruptured cerebral aneurysms in patients with polycystic kidney disease*. *Surg Neurol*. 62 (6), 2004, p. 538-45; discussion 545.

YASUI, T., SAKAMOTO, H., et al. *[Management of elderly patients with incidentally discovered unruptured aneurysms]*. *No Shinkei Geka*. 26 (8), 1998, p. 679-84.